Construction and Building Materials 270 (2021) 121475

Contents lists available at ScienceDirect

Construction and Building Materials

journal homepage: www.elsevier.com/locate/conbuildmat

Physical, chemical and mineralogical characterization of Dutch fine recycled concrete aggregates: A comparative study

Marija Nedeljković [a,b,*], Jeanette Visser [b], Timo G. Nijland [b], Siska Valcke [b], Erik Schlangen [a]

[a] Delft University of Technology, Faculty of Civil Engineering & Geosciences - Department of Materials & Environment, Stevinweg 1, 2628 CN Delft, the Netherlands
[b] TNO Buildings, Infrastructure & Maritime, PO Box 155, 2600 AD Delft, the Netherlands

HIGHLIGHTS

- The properties of individual and total fractions of fRCA were investigated.
- Based on combined experimental approaches, characteristic quality indicators were defined for fRCA.
- The content and surface area of fine fraction (0–0.250 mm) and particle size distribution of fRCA varied with the source.
- fRCA are made up by crystalline phases (>70 wt%), notably quartz (>60 wt%), and adhered cement paste (<30 wt%).
- Whether the unreacted binder particles in studied fRCA still represent any reactivity may be doubted.

ARTICLE INFO

Article history:
Received 30 June 2020
Received in revised form 8 October 2020
Accepted 22 October 2020
Available online 24 November 2020

Keywords:
Fine recycled concrete aggregates
Circular concrete
Mineralogy
Microscopic study
Quality indicators

ABSTRACT

In circular concrete design, beside cement replacement with more environmentally friendly cement types, there is also an urgent need for sand replacement with fine recycled concrete aggregates (fRCA). The variations in physical and chemical properties of fRCA and lack of standards for their quality evaluation are the main reasons for not yet using fRCA in new concrete.

In this study, an in-depth characterization of different Dutch fRCA is performed in order to examine suitability of fRCA as an alternative material for river sand and define indicators for fRCA quality. These indicators eventually can be related to concrete mix design and performance, so that fRCA can be classified as a material that can be used in structural concrete elements. This is achieved with physical, chemical and mineralogical characterization of individual and total fractions (0–0.250 mm, 0.250–4 mm and 0–4 mm). The physical properties such as grading, density, surface area, water absorption and cement paste content of fRCA were tested. The chemical analyses include quantification of element composition with X-ray fluorescence spectrometry (XRF) and carbonate content with thermogravimetry and mass spectrometry (TG-MS). Potential contamination (chlorides and sulfates) and reactivity of selected fractions were evaluated. In addition, qualitative and quantitative phase analyses with X-ray diffraction (XRD) combined with Rietveld refinement method were performed and supported by optical polarizing-and-fluorescence microscopic (PFM) study.

Based on combined experimental approaches, characteristic quality indicators were defined for fRCA. These indicators showed that fRCA were uncontaminated and nonreactive. Despite fRCA were from different origins, they had similar chemical and mineralogical composition and contained comparative chloride content. In contrast, the content and surface area of fine fraction (0–0.250 mm) and particle size distribution of fRCA varied with the source. With this it can be assumed that fRCA will have different effect on the properties of the new concrete.

1. Introduction

In the coming decade, sustainable construction materials with low environmental impact will have a crucial role in achieving a Circular Economy (CE). The Dutch CE strategy aims to make the Netherlands 'fully circular' by 2050 with an interim target of a 50% reduction of primary materials (minerals, fossil fuels and

* Corresponding author at: TNO Buildings, Infrastructure & Maritime, PO Box 155, 2600 AD Delft, the Netherlands and Delft University of Technology, Faculty of Civil Engineering & Geosciences - Department of Materials & Environment, Stevinweg 1, 2628 CN Delft, the Netherlands.
E-mail address: M.Nedeljkovic@tudelft.nl (M. Nedeljković).

https://doi.org/10.1016/j.conbuildmat.2020.121475
0950-0618/

metals) by 2030 [1]. Therefore, in the Netherlands, beside cement replacement with more environmentally friendly cement types, there is also an urgent need for circular materials for sand. Despite the potential that industrial waste has for concrete production, mainly as replacement for cement, resources for aggregates are not sufficient and concrete rubble is necessary to be included in the stream of alternative raw materials. The largest source of aggregates is the construction and demolition waste (C&DW) and its quantity will be significantly increasing due to aging and deterioration of the concrete infrastructure [2].

The variations in chemical and physical properties of fine recycled concrete aggregates (fRCA) [3,4], lack of experience, lack of standards for their quality evaluation, lack of existence of regular supply/demand systems and environmental concerns are the main reasons for fRCA being mainly used for low grade applications such as road pavements, sub-basements, soil stabilization, improvement of sub-ground [5,6]. However, this is not the most sustainable way of recycling, because the production of new concrete still requires large amounts of primary aggregates.

In some studies, parts of fRCA were used in cement raw meal for cement production [7,8]. Recent laboratory studies have shown the development of mortars and concretes with different fRCA replacement levels and the results related to their performances were encouraging [9,10]. However, the reuse of fRCA as a fine aggregate in new concrete have not been employed yet in practice. This is caused by the fact that concrete rubble has not been sorted at the source and therefore, recycled concrete aggregates might have large variations in the properties. The key question for application of fRCA as sand replacement in concrete is which properties would hamper the performance of concrete and, related to this, which quality indicators should be used.

Material characterization is an important step in order to understand variations of recycled material and their key properties affecting concrete performance. For example, the type of aggregate, or strictly speaking its modulus of elasticity, influences shrinkage of concrete, the particle size and shape influence workability and the mechanical properties of concrete [11]. Aggregate packing directly affects the way of aggregate particles forming a skeleton to transmit and distribute loads, thus influencing the stability and mechanical performance of the concrete. One of the most critical aspects for durability of concrete, are soluble chlorides and sulfates contained in concrete components of which the amount is limited in concrete in order to prevent degradation, in this case initiation of corrosion of reinforcement or sulfate attack. Typically, chlorides can be present in concrete components when cast, i.e. in water, cement, aggregates and in admixtures, but also concrete structures are often exposed to chloride-contaminated environments in the Netherlands, causing chloride ions to penetrate through the concrete cover [12]. After recycling of such a concrete, chemical composition and phase analysis can be an indicator for contamination/deterioration level of a recycled concrete. X-ray diffraction analysis (XRD) is a powerful tool in this regard, but challenges can arise due to the complex and often varying composition of fRCA. For this reason it is necessary to combine XRD with other characterization techniques such as thermogravimetry and microscopy studies. Up to now, the water absorption and water demand of fRCA are the most extensively and comprehensively studied among all properties of fRCA [13–16]. Only a few studies on physical–chemical-mineralogical characterization of C&DW recycled concrete aggregates including bricks [4,17] and of laboratory crushed concrete [18] have been done.

In the present study, characterization of physical properties, chemical and mineralogical composition of various Dutch fRCA (from unknown concrete rubble) is performed. The aim is not only to investigate properties of fRCA, but also to focus on how these properties (quality indicators) can be correlated to the mortar and concrete mix design with respect to the specific property of the mix. The physical analyses were performed with the following techniques: particle size distribution using a sieve tower and laser diffraction analyzer; density with helium gas pycnometer; BET specific surface area using a nitrogen adsorption. The chemical analyses consisted of: chemical analysis of acid-soluble chlorides and water-soluble sulfates; element composition measured with X-ray fluorescence spectrometry (XRF); carbonate content with thermogravimetry and mass spectrometry (TG-MS), isothermal calorimetry, X-ray diffraction analysis to characterize the crystalline phases; optical polarizing-and-fluorescence microscopy (PFM) to characterize mineralogy and morphology of fRCA.

2. Materials and methods

2.1. Materials

Three different fRCA were used in this study. They were chosen to be representative of major Dutch fRCA because of their geographical spread (B-fRCA is delivered from the South, C-fRCA is delivered from the West and D-fRCA from the East of the Netherlands) and recycling technique (jaw crusher combined with a cone crusher or rotor crusher). As reference material, Dutch river sand (A) with 93 wt.% of SiO_2 was used. All fRCA were first dried in an oven at 105 °C. The appearance of fresh and dry materials is shown in Fig. 1.

2.2. Physical properties testing

2.2.1. Particle size distribution and particle shape

After drying, fRCA were sieved and divided into eight fractions (<0.063 mm, 0.063–0.125 mm, 0.125–0.250 mm, 0.250–0.5 mm, 0.5–1 mm, 1–2 mm, 2–4 mm, >4 mm) using a sieve tower. After evaluation of individual fractions, it was decided to select two subfractions 0–0.250 mm and 0.250–4 mm and investigate their properties and compare to the properties of total fraction 0–4 mm (Fig. 2).

The particle size distribution for the fraction (0–0.250 mm) was measured using a laser diffractometer. In the tests, 0.5 g of sample powder was mixed with 800 mL ethanol (rather than water since hydration may take place when mixing cementitious material with water) and stirred for 5 min. Meanwhile, an ultrasonic vibrator was turned on to prevent agglomeration of fine particles. After mixing for 5 min, particle size measurement (distribution in volume) of fine powders was measured by laser. Three replicates were made per sample.

2.2.2. Density and specific surface area

Density of individual and total fractions (0–0.250 mm, 0.250–4 mm and 0–4 mm) was determined with a Helium Pycnometer (Model: Ultrapycnometer 1000), employing the method of gas displacement to measure volume accurately. Before the density measurements, the samples were dried and degassed at 105 °C until a constant mass in order to remove any trapped air and moisture. Ten consecutive volume measurements were performed to obtain an average density value. An average mass of the tested sample was 60 g.

Low temperature gas adsorption has been used to determine the surface area of river sand and fRCA. Next, the specific surface area is calculated by dividing absolute surface area of the sample by the sample mass. The specific surface area, S_BET, of fraction 0–0.250 mm was determined using nitrogen adsorption method based on Brunauer-Emmett-Teller (BET) theory [19]. The nitrogen adsorption tests were conducted by using Gemini VII 2390 with a relative pressure (P/P0) range from 0.05 ~ 0.99. The relative

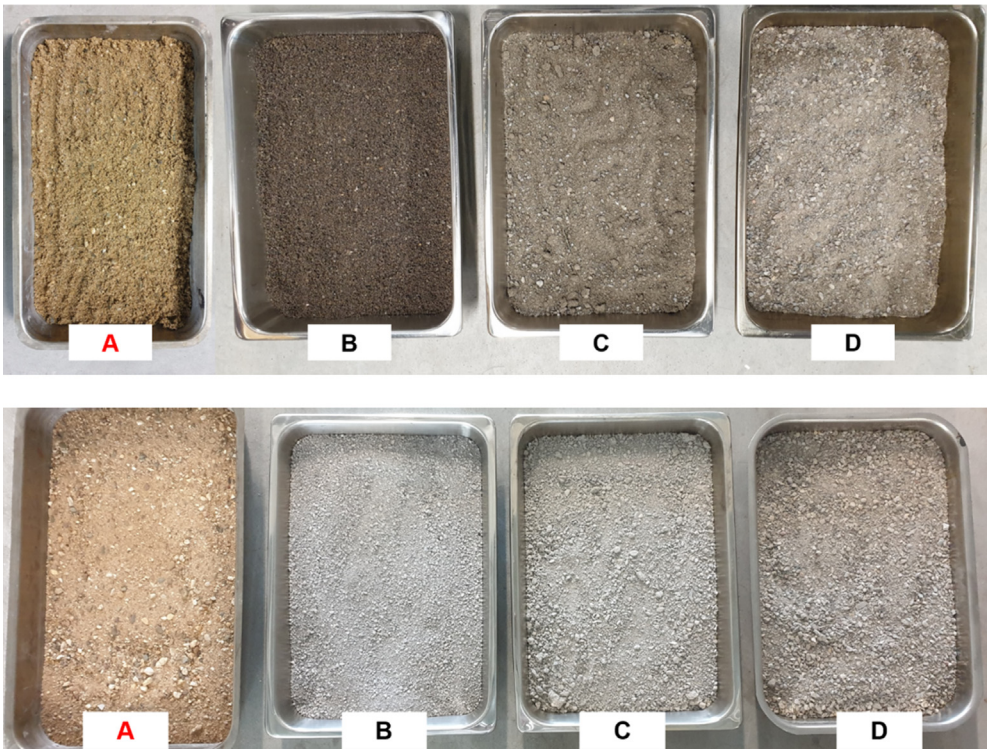

Fig. 1. River sand and fRCA before (top photo) and after (bottom photo) drying (river sand (A) and fRCA with different origins (B, C, D)).

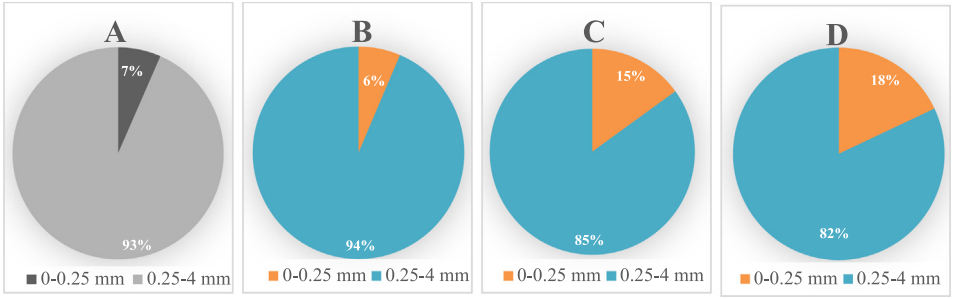

Fig. 2. The relative proportions (in wt.%) of particle size fractions (0–0.250 mm and 0.250–4 mm) of the 0–4 mm (river sand (A) and fRCA with different origins (B, C, D)).

pressure is defined as equilibrium vapor pressure divided by the saturation vapor pressure. Approximately 1 g of sample was used for the analysis.

2.2.3. Moisture content and water absorption

Materials were first dried in a ventilated oven at 105 °C until a constant mass to determine the moisture content according to NEN-EN 1097–5:2008 [20]. Constant mass is determined by successive weighings performed at least 1 h apart and not differing by>0.1%.

Water absorption of sands was determined according to standard NEN-EN 1097–6:2013 [21], by measuring the quantity of water present in the sands at saturated surface dry state (SSD).

2.3. Chemical-mineralogical properties testing

The procedure for extracting subsamples from fRCA (0–4 mm) was followed from NEN-EN 932–2:1999 [22] for chemical–mineralogical analysis. The original amount of samples was about 20 kg for each batch. Of this, a subsample of about 3 kg was taken according to NEN-EN 932–2. For the grain size fraction 0–4 mm, the standard requires a minimum of 0.5 kg. The amount of 3 kg is taken as a representative amount in relation to the possible inhomogeneous distribution of any fRCA particles, and inhomogeneous distribution of any relevant chemical elements in them. For XRF, TG-MS and XRD analyses, the fRCA samples were first ground with a grinding machine (a Fritsch pulverizer 5) to an average particle size of 100 μm. After grinding, milling with an Alpine e200 LS air jet sieve of fRCA fractions was done and particles with an average size of 25 μm were obtained. This powder was used for XRD and TG-MS analyses. Additional manual grinding down to an average size of 10 μm was done for XRF analysis. For analyses of acid-soluble chlorides, water-soluble sulfates, calorimetry and microscopic study, samples were not ground.

2.3.1. Acid-soluble chlorides and water-soluble sulfates

The acid-soluble chlorides were obtained by acid dissolution using 6 M nitric acid according to NEN-EN 1744–5:2006 [23]. As this standard is designed for samples with a much lower weight and much higher chloride concentration, representativity may be a problem for the fRCA samples. Therefore, quantities of test specimens were modified. Samples of ca. 20 g were used. Acid-soluble

chloride salts content was further determined following Volhard method cf. NEN-EN 1744–5:2006. The solid residue left on the filter paper was dried in an oven at 105 °C for 24 h. This allowed determination of the cement paste content by subtracting the weight of insoluble substances from the initial weight of the oven-dried material.

The water-soluble sulfate content in the fRCA was determined according to NEN-EN 1744–1:2009 +A1:2012 § 10.2 [24]. The sample consisting of 25 g of sand (crushed below 4 mm) was mixed with 1 L of water at 65 °C under stirring to extract water-soluble sulfate ions. A neat sample is filtered using a Buchner filter with a medium grade filter paper 110, and the filtrate is analyzed by Metrohm 850 ion chromatography system. Sulfate ion was resolved on an anion exchange column and detected by a conductivity detector. Quantification was performed by linear regression analysis of peak areas from the standard sulfate calibration curve containing five points.

2.3.2. X-ray fluorescence spectrometry

The X-ray fluorescence spectra of studied materials were recorded with a Bruker S8 Tiger spectrometer on pressed pellets. As binding agent, Boreox ($C_{12}H_{22}O_{11}$) from Fluxana, was used. Samples were mixed in a stainless steel grinding cup. The loss on ignition (LOI) was measured by heating the fRCA to 1050 °C. The LOI is expressed in weight percent of the dry matter [25]. The mass of the sample was 5 ± 0.1 g.

2.3.3. Thermogravimetric-mass spectrometric analysis

A TGA (Netzsch STA 449 F3 Jupiter) coupled with a Netzsch QMS 403C mass spectrometer was used to quantify H_2O and CO_2. Samples of circa 35 ± 0.5 mg were placed in an alumina crucible and exposed under an inert atmosphere of argon and increasing temperatures ranging from 40 °C to 1050 °C at a heating rate of 10 °C/min. A blank curve, obtained under the same conditions with the same empty alumina crucible, was systematically subtracted.

The mass spectrometer was coupled to the TG to allow separation of concurrent mass loss from H_2O and CO_2 releases, which were compared to a standard sample with known concentration (in this case calcite and gypsum) under identical analytical conditions [26]. The peak integral, i.e. the area under the MS H_2O and CO_2 curves, was quantified using OriginPro 9 software for each sample.

2.3.4. Isothermal calorimetry

The fRCA may contain unreacted binder particles which in contact with water may dissolve and react. Isothermal calorimetry analysis was carried out to investigate possible reactivity of unreacted binder particles. Fines under 0.250 mm were used for experiments, since cement paste has a tendency to accumulate in the finest fractions. The control sample was cement paste, CEM I 42.5 N with water-to-cement ratio 0.5. All the raw materials were conditioned at the measurement temperature. Samples were prepared outside the calorimeter. Water was added to fines in order to study their reactivity (water-to-fines ratio 0.5). For a calorimetry test, the sample (mix of water and fines) is stored in a glass ampoule (125 mL) and placed in the calorimeter (3-channel TAM Air, Thermometric). The content of fines was 28.8 g. The calorimeter consists of 3 parallel twin type measurement channels: one from the sample, the other for the reference. A glass ampoule with water was used as a reference. Once the thermal equilibrium is reached, the heat evolution is recorded at the constant temperature (20 °C). Three replicates were measured simultaneously.

2.3.5. X-ray powder diffraction and rietveld refinement analysis

Diffractograms of studied materials were recorded using a Bruker D8 Advance X-ray powder diffractometer, equipped with LynxEye detector. The machine was operated with an accelerating voltage of 40 kV and an X-ray beam current of 40 mA. The X-ray source was a Cu-tube working with characteristic Cu-Kα wavelength of 1.54060 Å. The samples were scanned varying the 2-theta angles between 10° and 70°. For quantitative phase analysis, standard reference material (alumina, Al_2O_3, NIST Standard Reference Material 676a) was added and mixed for about 2 min. Phase identification was performed using Bruker Eva 4.2 software and appropriate databases. Rietveld quantitative phase analysis was performed using Bruker Topas 5.1 software.

2.3.6. Optical polarizing-and-fluorescence microscopy (PFM)

Mineralogical composition of fRCA is important since it can have both positive and negative impacts on the concrete properties if aggregates are altered/deteriorated as to unstable silica phases. Therefore, PFM study was performed to identify components present (clinker phases, supplementary cementitious materials (SCMs), reaction products like portlandite, ettringite), and any internal debonding, microcracking and deterioration processes (e.g. carbonation, ASR, sulfate attack), morphology of aggregates and the presence of any other materials (e.g. fibers), following the approach of Nijland and Larbi [27].

Twelve thin sections were made and examined in plane-polarized and cross-polarized transmitted light at magnifications up to × 400.

Sample preparation is based on Dutch CUR recommendation 89 [28]. The materials (0–4 mm) were sieved to prepare two groups of samples, respectively, sized 0.063–2 mm and 2–4 mm. The representative grains were chosen for each group (group I: 0.063–2 mm, group II: 2–4 mm).

Sample preparation consists of the following steps:

- drying at 105 °C to constant mass;
- quartering the dried sample cf. NEN-EN 932–2:1999 [22];
- sieving one quarter into three fractions: 0–2, 2–4 and > 4;
- crushing the fraction > 4 mm to a maximum grain size of 4 mm;
- sieving this fraction into three fractions: < 0.063 mm, 0.063–2 mm and 2–4 mm;
- weighing the homogenised fractions 0.063–2 mm and 2–4 mm;
- for the fraction 0.063–2 mm and 2–4 mm, taking representative subsamples for one and two thin sections per fraction, respectively.

3. Results

In this section, first, the characterization of the physical properties is presented, followed by the chemical characterization. Subsequently, mineralogy was determined by XRD and microscopy. Finally, fRCA particles are evaluated with optical polarizing-and-fluorescence microscopy.

3.1. Physical properties

3.1.1. Appearances of fRCA

Aggregate shape and surface texture affect concrete mix workability and adhesion of the cement paste, respectively. An overview of different fRCA fractions are presented in Fig. 3. The smaller fractions show more homogeneous shapes. Visual observations of larger size particles show that the shape of the particles varies from round to angular. The key observations are:

–the variation of particle morphology and colour within a particle population is low, –the variation of particle morphology and colour between river sand and fRCA is high because the fRCA has particles with high sphericity to angular or sub-angular with low sphericity cf. Power's scale of roundness [29]; and the presence of cement mortar in fRCA, –the variation of particle morphology

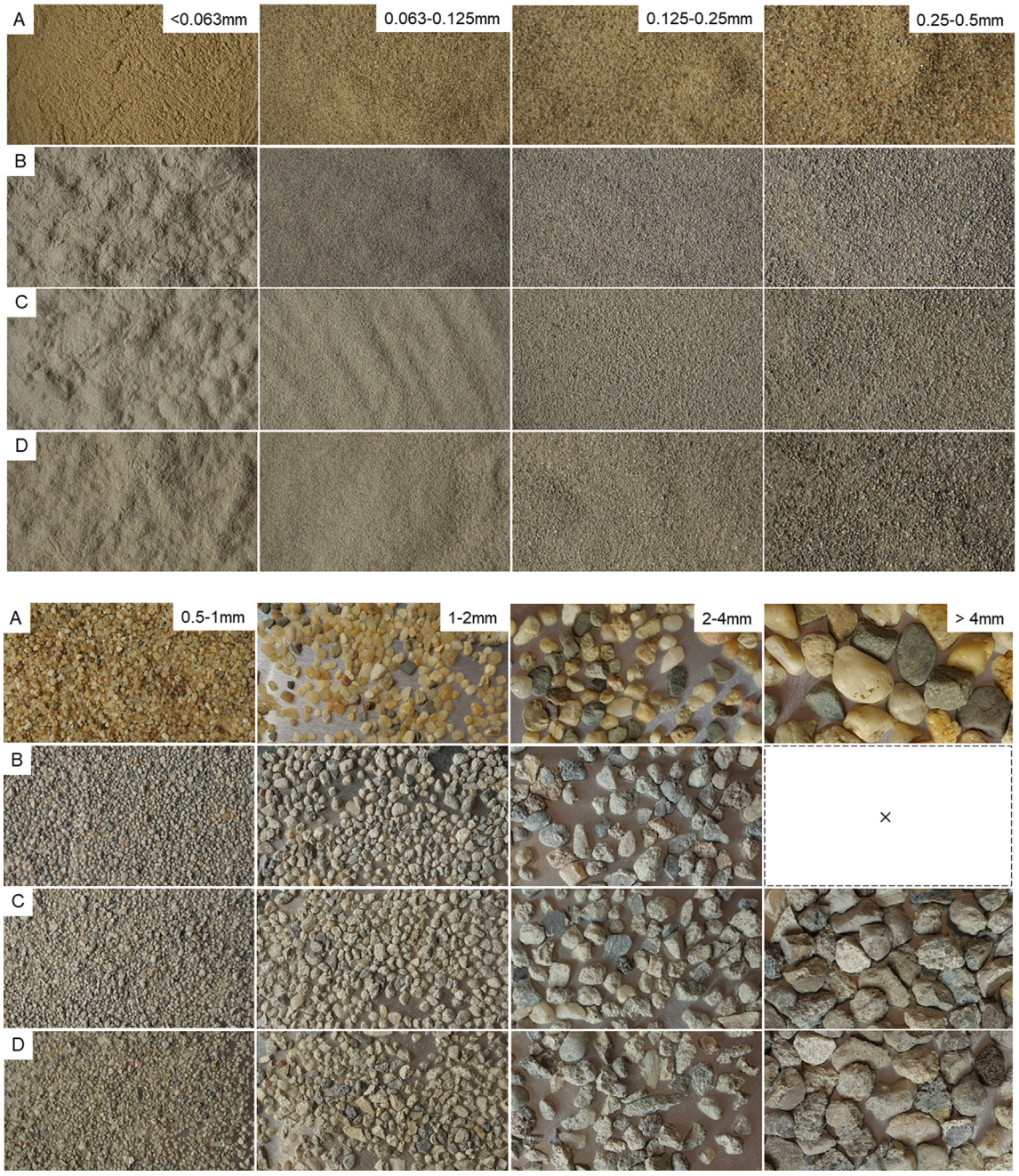

Fig. 3. Overview of particle morphology and colour of river sand (A) and three different fRCA (B, C, D) for various particle populations.

between different fRCA (B, C, D) is small compared to that between fRCA and reference sand (Fig. 4), –the variation in colour of sub-fractions in the range 0–0.5 mm is high in Fig. 3: each batch is defined by a different colour.

Contaminants in fRCA are<5% and include wood, iron/steel, different plastics and polymers, glass and plant fibers as identified by stereomicroscopy.

3.1.2. Grading curves and standard limits of sand

The aggregate grading is an important characteristic as it affects, amongst others, workability and packing density of the concrete mix. The particle size distribution of different fRCA with range 0–4 mm is shown in Fig. 5. In addition, lower and upper limits according to NEN-EN 12620:2002+A1:2008 [30] are shown for assessment of the suitability of fRCA for use as a sand for concrete mix design. The fRCA from different batches complies with the overall limits in NEN-EN 12620:2002+A1:2008 [30].

Variations in particle size distributions between three samples within the same batch is low, meaning that tested samples are representative for a single batch. On the other hand, the variations of particle size distributions (S-shape) between different fRCA (B, C and D) is high (Fig. 5).

The different percentages for grain size fractions of different fRCA, like the higher percentages of fraction 0–0.250 mm in C and D (15–18 wt%) compared to B (~6 wt%) (Fig. 6) may be due to the number of crushing steps applied during recycling. For instance, source B has one step of crushing in the process, while C and D have three steps.

The particle size distribution of sands of particles sizes 0–0.250 mm analyzed by laser diffraction, is shown in Fig. 7. The

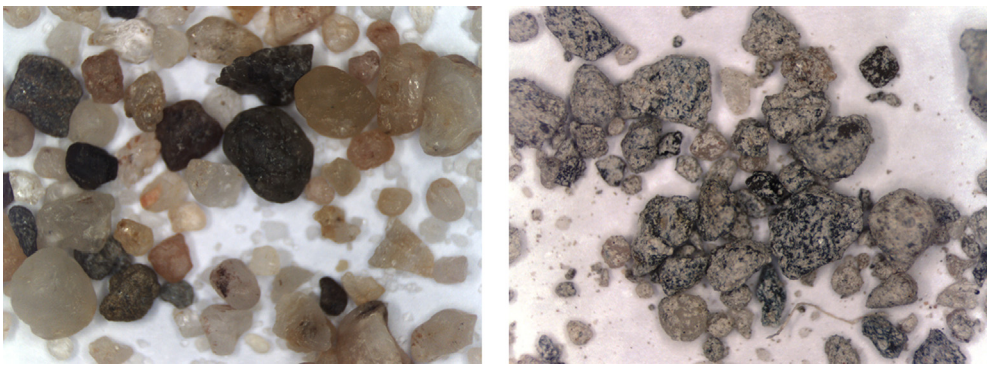

Fig. 4. Microscopic observation of river sand A (left) and fRCA C (right), particle population 2–4 mm.

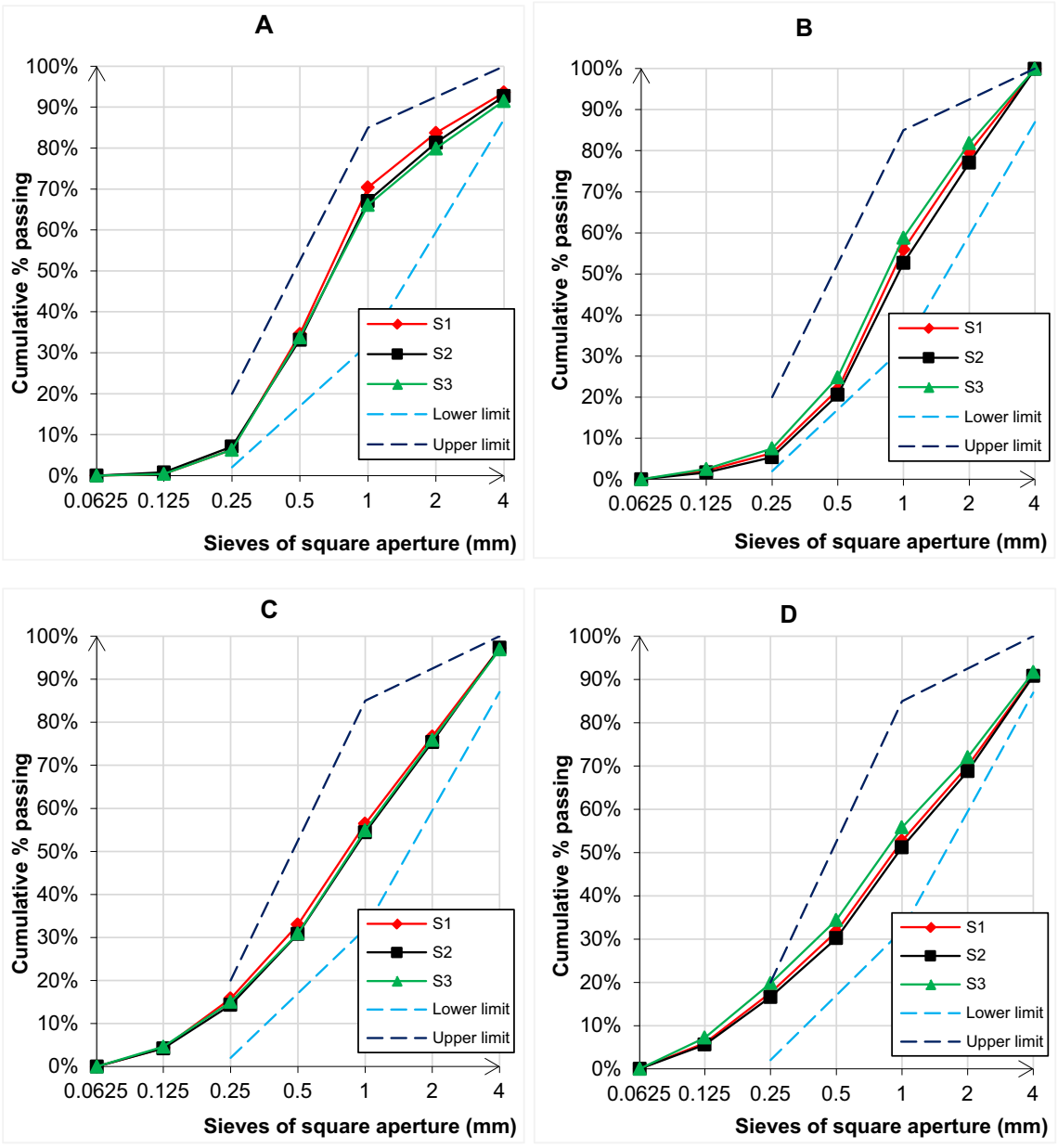

Fig. 5. Particle size distributions of river and fRCA, 0–4 mm, obtained by dry sieving method, upper and lower limits according to NEN-EN 12,620 [30].

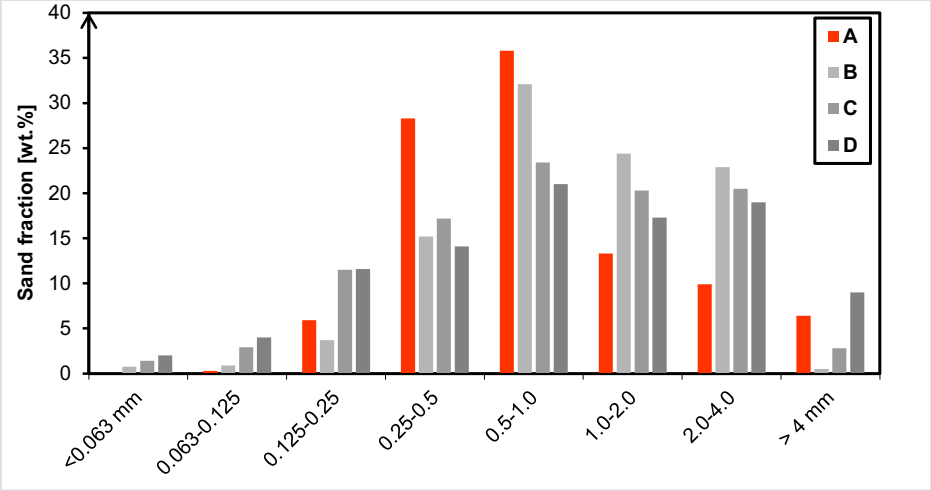

Fig. 6. Fractioning of river sand (A) and fRCA (B, C and D).

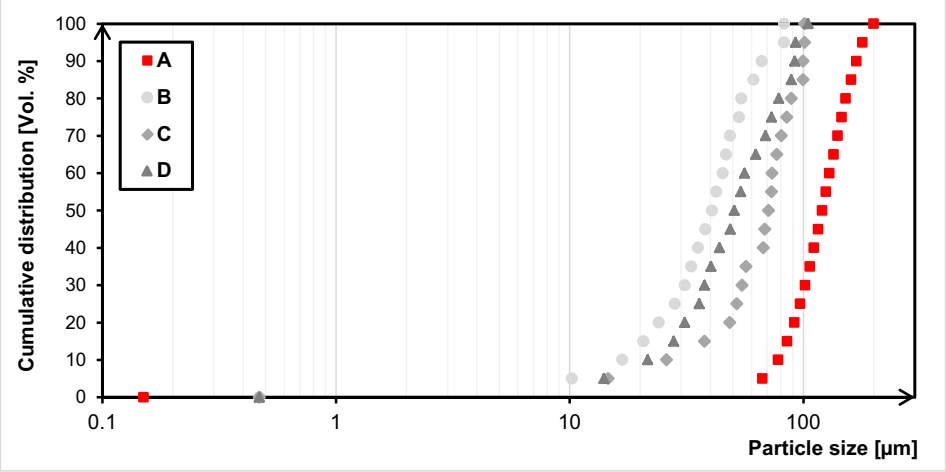

Fig. 7. Cumulative particle size distributions of river sand and fRCA, 0–0.250 mm, analyzed by laser diffraction using ethanol as dispersion medium.

fRCA, with a dominantly angular shape, has finer particle size distributions compared to river sand (A). It is interesting to note that median size of fRCA is larger compared to some of industrial by-products such as fly ash, ground granulated blast furnace slag or metakaolin, but similar to that of CEM I 42.5 N and limestone powder (Table 1).

Table 1
D_{50}- particle size [µm] of different materials 0–0.250 mm, obtained by laser diffraction and BET surface area [m^2/g] obtained by N_2 adsorption.

Material	D_{50} (µm)	BET surface area [m^2/g]
CEM I 42.5 N	44.5[31]	0.8[31]
CEM III/B 42.5 N	22.0	
Fly ash	21.0[32]	1.7[33]
Ground granulated blast furnace slag	19.0[32]	2.5[33]
Metakaoline	11.5[34]	
Limestone powder	34.6[31]	0.75[31]
Micronized sand M300	23.9[31]	1.2[31]
A	125	0.7
B	41	8.9
C	71	6.4
D	50	7.8

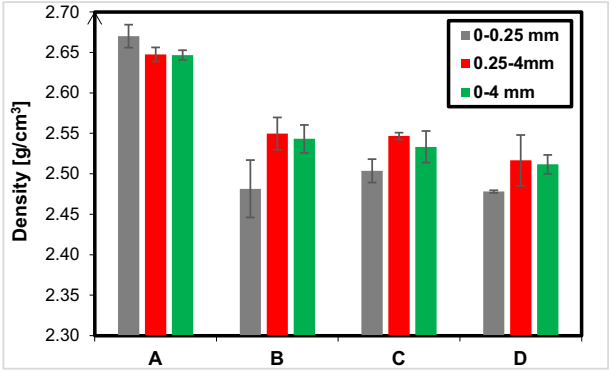

Fig. 8. Density of river sand (A) and fRCA (B, C, D).

3.1.1. Density and specific surface area

Fig. 8 shows density results. For every fraction of fRCA (B, C, D) the density is lower than for river sand fraction (A); the largest difference occurs in the finest fraction, i.e. 0–0.250 mm. Typically, density of quartz and hardened cement paste are 2.65 g/cm^3 and 1.5–2.2 g/cm^3, respectively. The density of fRCA is reduced

compared to density of pure quartz, but it is higher than that of pure cement paste.

The BET specific surface area was measured for the fraction 0–0.250 mm (Table 1). fRCA has much higher specific surface areas than river sand. The BET specific surface area of fRCA is higher than BET values of cement, slag, fly ash and fillers (Table 1), but similar to those found by [35]. This high BET specific surface area of fRCA is likely due to presence of calcium silicate hydrate (CSH) phase in mortar adhered to sand particles. CSH has high specific surface areas ranging from 30-112 m^2/g [36]. Furthermore, particle size distribution also differs between different fRCA (B, C, D) (Fig. 7) and affects their specific surface areas.

3.1.2. Moisture content and water absorption

Fig. 9a shows moisture content of river sand and fRCA upon delivery. The fRCA B has the highest free water content. The moisture content of studied fRCA was similar to that of studied fRCA by Lotfi et al. [37], which was 12 wt.%. Fig. 9b shows the large difference in water absorption between river sand and fRCA, the latter similar to values found by Ulsen et al. [38].

3.2. Chemical properties

3.2.1. Cement paste, chlorides and sulfates

Table 2 lists cement paste content, chlorides and sulfates in different fractions. Content of old cement paste adhered to the fRCA ranges from 14 wt.% to 29.8 wt.%, depending on the batch (B, C, D) and particle size (0–0.250 mm, 0.250–4 mm, 0–4 mm). These are comparable to cement paste contents 16.1 wt.% and 24.6 wt.% for recycled coarse and fine concrete aggregates, respectively [4]. The cement paste concentrates in the finer fraction (0–0.250 mm), in agreement with [38].

In contrast to river sand (A), fRCA contains chlorides and sulfates (Table 2). fRCA C has a higher Cl^- content than batches B and D (Table 2). The water soluble sulfates content in the fRCA is below standard limit value 0.2 wt.% (NEN-EN 12620:2002 +A1:2008) [30], except for B 0–0.250 mm and D 0–0.250 mm. The high water soluble sulfates of fRCA B 0–0.250 mm and D 0–0.250 mm might be due to various causes, including breakdown of ettringite due to carbonation of cement paste [39] or contamination by gypsum.

Table 2
Cement paste content, acid soluble Cl^- and water soluble SO_4^{2-} in fRCA.

	Cement paste [wt.% of dry sample]	Acid soluble Cl^- [wt.% of dry sample]	Water soluble SO_4^{2-} [wt.% of dry sample]
A			
0–0.25 mm	0.00	0.00	0.01
0.25–4 mm	0.00	0.00	0.00
0–4 mm	0.00	0.00	0.00
B			
0–0.25 mm	28.9	0.04	0.37
0.25–4 mm	17.9	0.04	0.14
0–4 mm	19.0	0.04	0.16
C			
0–0.25 mm	29.8	0.06	0.18
0.25–4 mm	21.4	0.05	0.09
0–4 mm	25.8	0.04	0.14
D			
0–0.25 mm	22.7	0.04	0.24
0.25–4 mm	14.7	0.04	0.08
0–4 mm	16.2	0.04	0.10

3.2.2. Bulk chemical composition

The bulk chemical composition of the different grain size fractions is given in Table 3, expressed as oxides. The river sand is composed mainly of >93 wt.% SiO_2 and minor CaO, Al_2O_3, MgO, K_2O, Fe_2O_3 and total sulfur expressed as SO_3. fRCA is made up mainly by SiO_2 (62–76 wt.%), CaO (14–23 wt.%), Al_2O_3 (6–10 wt.%) and Fe_2O_3 (1.6–3.3 wt.%). In comparison to river sand, the fRCA contain lower amounts of SiO_2 and higher amounts of CaO, Al_2O_3, MgO, K_2O, Fe_2O_3, SO_3. This is due to presence of old cement paste in fRCA. The fraction 0–0.250 mm has a different composition compared to 0.250–4 and 0–4 mm with a reduced SiO_2 content (59–67 wt.%) and increased CaO (19–27 wt.%). The LOI was 8–11 wt.%.

3.2.3. TG-MS

Fig. 10 shows the TG-DTG curves for different fRCA. In addition, the MS H_2O and MS CO_2 curves of materials are plotted in Fig. 11. Using MS curves, the precise temperature ranges for H_2O and CO_2 emission can be determined. Using both the MS and TG-DTG curves, enables the weight loss calculation. After distinction between H_2O and CO_2, content of $Ca(OH)_2$ and $CaCO_3$ could be determined based on the independent decomposition reactions for $Ca(OH)_2$ and $CaCO_3$, according to the equations:

$$w_{(Ca(OH)_2)} = w_{(H_2O)} \times \frac{74g/mol}{18g/mol} \quad (1)$$

$$w_{(CaCO_3)} = w_{(CO_2)} \times \frac{100g/mol}{44g/mol} \quad (2)$$

where $w_{(H_2O)}$ and $w_{(CO_2)}$ are the weight losses determined by TG-MS.

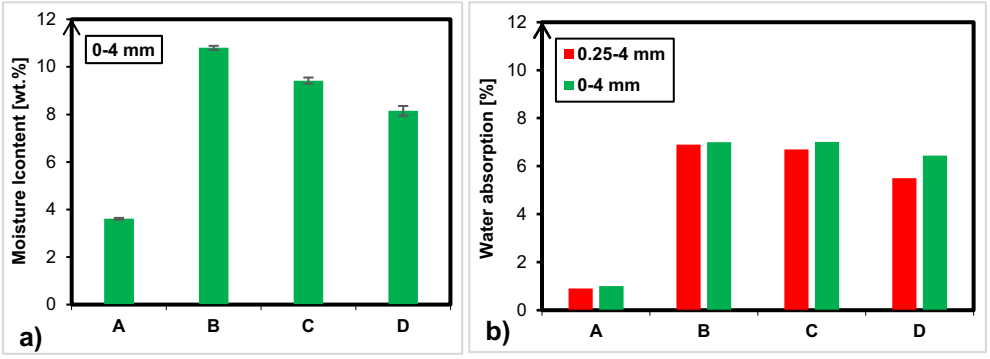

Fig. 9. a) Moisture content of 0-4 mm of river sand (A) and fRCA (B, C, D); b) Water absorption after 24 h of 0.250-4 mm and 0-4 mm of river sand (A) and fRCA (B, C, D).

Table 3
Bulk chemical composition of different fractions of river sand and fRCA.

	SiO_2	CaO	Al_2O_3	MgO	Na_2O	K_2O	TiO_2	Fe_2O_3	SO_3	Cl
A										
0–0.25	93.6	1.1	2.5	0.2	0.5	0.9	0.2	0.9	0.04	0.00
0.25–4	95.6	0.9	1.7	0.1	0.2	0.7	0.1	0.5	0.08	0.00
0–4	96.0	0.5	1.8	0.1	0.2	0.7	0.1	0.5	0.05	0.00
B										
0–0.25	67.8	19.1	5.2	1.2	0.6	1.3	0.4	3.1	0.97	0.03
0.25–4	70.3	17.1	5.1	1.4	0.6	1.3	0.4	2.6	0.98	0.03
0–4	62.8	22.5	5.8	1.5	0.6	1.5	0.5	3.3	1.16	0.03
C										
0–0.25	58.6	27.5	5.1	2.1	0.6	1.5	0.4	2.4	1.32	0.10
0.25–4	62.7	25.8	4.1	1.5	0.4	1.3	0.3	2.4	1.00	0.09
0–4	68.2	20.4	4.4	1.6	0.5	1.2	0.3	2.0	0.91	0.07
D										
0–0.25	59.5	26.7	5.8	1.3	0.5	1.5	0.4	2.4	1.56	0.06
0.25–4	71.7	17.3	4.8	1.1	0.4	1.1	0.3	2.0	1.12	0.04
0–4	75.8	14.4	4.3	0.9	0.4	1.1	0.3	1.7	0.89	0.04

Note: All XRF results, except Cl, are expressed as oxides, i.e. the SO_3 represents total sulfur (both sulfate and sulfide).

Fig. 10 shows a three-stage weight loss in the TGA-DTG curves of fRCA samples. The first stage is due to the evaporation of physically and chemically bound H_2O from CSH, monosulfate and ettringite between 105 and 430 °C. The second stage of weight loss from 410 to 480 °C is due to dehydroxylation of $Ca(OH)_2$. The third stage can be divided to: a substage 250–700 °C due to further dehydration of CSH [40,41] and decomposition of amorphous carbonates and semi-crystalline carbonates, and a substage 700–925 °C due to decomposition of crystalline carbonates. The major weight loss was due to CO_2 emission and therefore carbonates decomposition. All fractions (except fraction 0–0.250 mm in fRCA (B)) have the characteristic peak for CO_2 emission at 775 °C, suggesting the same origin of CO_2 regardless the batch (B, C, D) being calcite. Less strongly held CO_2 molecules in fraction 0–0.250 mm in fRCA (B) suggest presence of less stable forms of $CaCO_3$, such either amorphous or the polymorphs vaterite and aragonite. The temperature range for main H_2O emission is the same for all fractions, with the exception of the peak shape which is different. For batch (B), the peak for H_2O emission is more narrow than for batches (C) and (D), suggesting different type (structures) of reaction products. From TG-MS H_2O, it is clear that portlandite is present still in some of fRCA, its amount not exceeding 2 wt.% as shown in Table 4.

Table 4 gives the overview of temperature ranges and corresponding weight loss for H_2O and CO_2, but also the total weight loss and content of $Ca(OH)_2$ and $CaCO_3$. Table 4 shows that there was more H_2O released from fraction 0–0.250 mm, compared to other two fractions. This is due to larger cement paste content in fraction 0–0.250 mm (Table 2) and therefore, more hydration products containing physically and chemically bound water. The CO_2 content presents sum of physically and chemically bound CO_2. The $CaCO_3$ content presents the sum of Ca-carbonates (amorphous, vaterite, aragonite, calcite), limestone filler and aggregate (and any other carbonate bearing aggregates), shown to be present by PFM study (section 3.3.2).

Reactivity of unreacted binder particles

The comparison of normalized heat release rate and cumulative heat between the cement paste and different fRCA (0–0.250 mm) is shown in Fig. 12 and Fig. 13. The hydration of cement shows two reaction stages (two calorimetric peaks) that are controlled by different reaction mechanisms (Fig. 12a). The first calorimetric peak, occurring within the first few minutes, mainly reflected the initial wetting/dissolution of cement. The second calorimetric peak, occurring after around 6 to 24 h, reflected the formation of hydration products. Fig. 12b presents only a small initial peak for all types of fRCA (B, C, D) compared to cement hydration kinetics (Fig. 12a). Based on the total cumulative heat results (Fig. 13), the reactivity of fRCA (from sources B/C/D) is negligible (<0.7 J/g of sand) compared to reactivity of cement (91.1 J/g of cement).

3.3. Mineralogical characterization

3.3.1. XRD

Fig. 14 shows the X-ray diffractograms of investigated river sand and fRCA, while Table 5 gives an overview of the phases combined with quantification using Rietveld refinement method. It is apparent that total fraction and subfractions within each batch contain the same phases (Fig. 14). The main phases of fRCA are quartz and calcite. Besides quartz and calcite, albite, orthoclase and microcline are present in all aggregates; quartz makes up 60 wt.% (Table 5). Besides dolomite which is also observed in batch C, there were no other phases present in the fRCA. The amount of quartz is significantly less in the fRCA (B, C, D) compared to river sand (A). Each of the phases, their origin and content, is presented next.

Quartz. Occurring in all three fRCA (B, C, D) in high amounts, deriving from the original aggregate which is usually siliceous river or marine sand.

Calcite. Potentially derived from one of the following sources: aggregates (limestone, carbonate cemented sandstone; also the source of dolomite) and carbonation of cement hydrates either during concrete service life or after demolition and crushing of concrete.

Furthermore, Table 5 gives the total content of amorphous phase that is likely to be composed of amorphous hydration products in cement paste (e.g. CSH), unreacted binder components (such as slag, fly ash, amorphous clinker) and amorphous $CaCO_3$ from carbonation of fRCA. Unhydrated cement clinkers were not identified within the XRD detection limit.

3.3.2. Microscopic investigation

3.3.2.1. Mineralogy of aggregates. In Fig. 15, an overview is given of the grain size fractions 0.063–2 mm and 2–4 mm for river sand and different fRCA (B, C, D). Particles of river sand are generally (sub) rounded while fRCA are more angular and often composite (Fig. 15). In the fRCA, the visual bonding between cement paste and aggregates is variable, from good to lack of adhesion as is the thickness of cement paste around natural aggregate grains.

For fRCA 2–4 mm, four types of representative particles are distinguished (Fig. 15i):

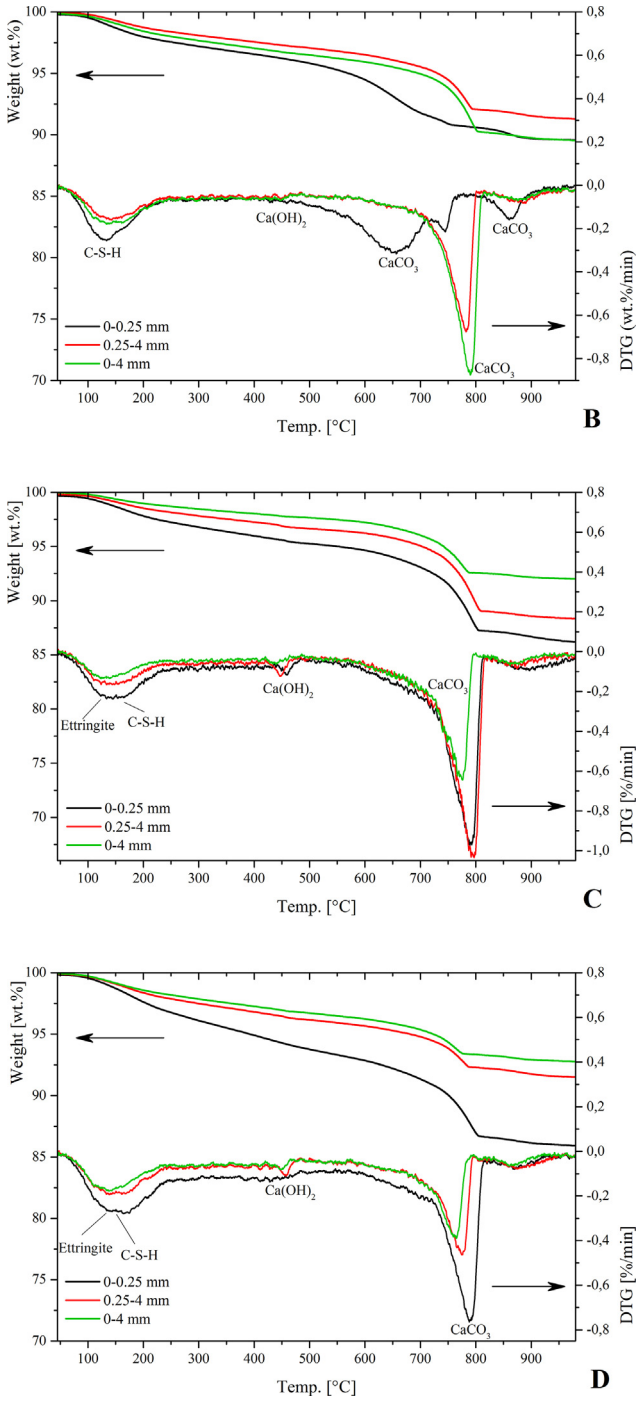

Fig. 10. TGA and DTG curves for fRCA (B, C, D).

- type I: Single aggregate particles. Those are original aggregate grains, either monomineralic grains or lithic fragments, in the range of 2–4 mm. This type is mostly made up by quartz and calcite (in limestone), whereas feldspars (plagioclase and K-feldspar (including microcline), mica, pyroxenes (in the basalt aggregate) and accessoria common in Dutch river sand (e.g. glauconite, tourmaline) also occur;
- type II: Low/high amount of cement paste adhered to one aggregate grain;
- type III: Dense cluster of particles (several aggregates linked by cement paste). The original aggregate grains are homogenously distributed in the cement paste (Fig. 16). In general, two subtypes can be distinguished:
  - particles of smaller (below 2 mm) and bigger (2–4 mm) sizes and different shapes in a confined space linked by cement paste,
  - particles of smaller sizes than 2 mm and different shapes in a confined space linked by cement paste;
- type IV: Loose cluster of particles, i.e. with a high aggregate-to-binder ratio, large amount of voids and poor internal coherence (Fig. 16). Their microstructure resembles that of a bedding or pointing mortar or plaster rather than concrete. In general, type IV particles contain two groups of particles:
  - particles of smaller sizes (below 2 mm) and bigger (2–4 mm),
  - particles of smaller sizes than 2 mm and different shapes in a confined space linked by cement paste.

For fRCA 0.063–2 mm, three types of representative particles are distinguished (Fig. 15ii):

- type I: Single aggregate particles, as in the 2–4 fraction, but in the range of 0.063–2 mm.
- type II: Several aggregate particles linked with cement paste, usually in a dense cluster of particles (as type III in the 2–4 fraction); in the fRCA 0.063–2 mm fraction, nearly all voids in these particles are clean, without any phases such as portlandite or ettringite.
- type III: Mortar particles, with a low content of aggregates and high content of cement paste.

Fig. 17i shows fRCA with a weak cohesion between aggregate particles and cement paste, an example of poorly compacted concrete. In contrast, Fig. 17ii shows fRCA with strong bond between the hardened cement paste and sand particles.

The microphotographs in Fig. 18 show that the limestone is present in variable amount in each thin section, which may be up to about 10 wt.% of the aggregate. It originates from the aggregate source of the parent concrete. A small number of fired clay brick particles were also observed in fRCA.

The interfacial zone between aggregate and cement paste is often considered the weakest part of normal concrete, being the most feasible part for crack initiation and propagation. An example of an open aggregate-cement paste interface is shown in Fig. 19. However, such open interfaces are negligible in fRCA; the interfacial zone between cement paste and original aggregate is visually good (Fig. 20). Nevertheless, different ITZs will be present in microstructure of hardened mortars and concretes with fRCA due to compositional differences among fRCA. In addition to compositional differences, differences in porosity of the adhered cement paste will also cause different ITZs. Some (entrapped) air voids and irregular voids due to lack of compaction are also present.

3.3.2.2. Mineralogical composition of old cement paste. As might be expected, unreacted binder components common in the Netherlands such as Portland clinker, slag, fly ash and limestone filler are encountered in the old cement paste.

Fig. 21 shows an example of calcium silicates (C_3S and C_2S). Similarly, Fig. 21 shows the unreacted slag in old cement paste typically 20–100 μm in size with well-developed microstructure of the cement paste. Unreacted fly ash spheres were also observed. The cement paste also contains occasional secondary reaction products. Minor amounts of undeleterious secondary ettringite were found in some air voids of fRCA (D batch) in the fraction 2–4 mm (Fig. 21). Fig. 22 shows the presence of limestone filler particles (B batch) with irregular shapes in the cement paste.

More important than the minor ettringite is carbonation of the cement paste, either during the service life of the parent concrete (Fig. 23), or, in case of the very thin outermost rim on the particles, during the storage after recycling of the parent concrete (Fig. 24).

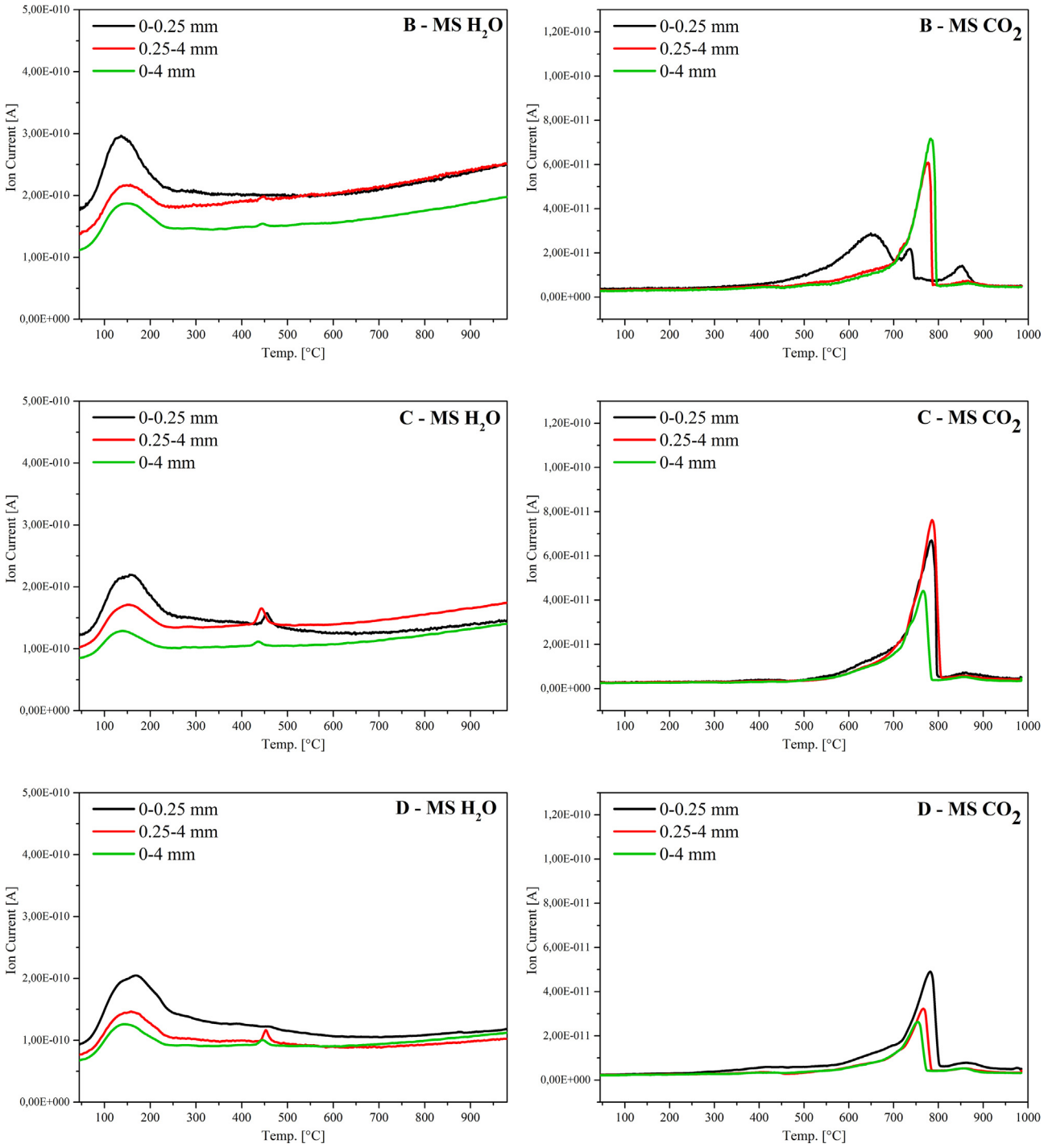

Fig. 11. MS H_2O and CO_2 ion currents used for determination of temperature ranges for calculation of individual weight losses due to H_2O, OH^- and CO_2.

4. Implications of characterization

Prior work has documented the use of fRCA, as sustainable alternative to natural sand, in the concrete. This concrete may exhibit similar or distinctive behavior from mortars/concretes with natural sand depending on the water absorption capacity of fRCA [15,16,42–45]. However, these studies have not focused on other properties which might also influence the performance of concrete and should be considered for appropriate concrete mix designs with fRCA. In this study, comprehensive characterization of the three types of fRCA has been done. The results have important implications for future concrete mix designs with fRCA.

Table 6 gives an overview of several physical, chemical and mineralogical quality indicators for fRCA in comparison to river sand. The indicators are: particle shape, particle size distribution, content of fraction 0–0.250 mm, density, specific surface area (BET), water absorption, Cl^- and SO_4^{2-} content, mineralogy of fRCA, cement paste content, milling time to complete crushing. Each of these indicators can be correlated to the concrete mix design with respect to the specific property of the mix.

Table 4
H_2O, CO_2, total weight loss, $Ca(OH)_2$ contents in fRCA measured by TG-MS technique.

	H_2O in CSH and other hydration products		H_2O in $Ca(OH)_2$		CO_2 (as physically and chemically bound)				
	MS	TG	MS	TG	MS	TG	Total	$Ca(OH)_2$	$CaCO_3$
	Temp.range[°C]	loss[wt.%]	Temp.range[°C]	loss[wt.%]	Temp.range[°C]	loss[wt.%]	loss[wt.%]	[wt.%]	[wt.%]
B	105–430		410–480		250–925				
0–0.25 mm		3.32		0.00		6.79	10.11	0.00	15.43
0.25–4 mm		2.66		0.13		5.75	8.54	0.53	13.07
0–4 mm		3.00		0.22		6.99	10.21	0.90	15.89
C									
0–0.25 mm		3.93		0.40		8.73	13.06	1.64	19.84
0.25–4 mm		2.55		0.48		8.18	11.21	1.97	18.59
0–4 mm		1.97		0.26		5.58	7.81	1.07	12.68
D									
0–0.25 mm		3.72		0.00		10.34	14.06	0.00	23.50
0.25–4 mm		3.30		0.38		4.64	8.32	1.56	10.55
0–4 mm		2.81		0.32		3.98	7.11	1.32	9.05

Note: Sum of individual weight losses (second, third, fourth column) is equal to the total weight loss (fifth column). The individual weight losses can be only calculated with combined TG-MS analysis. The total weight loss can be then compared to the total loss which can be determined from the TG curves.

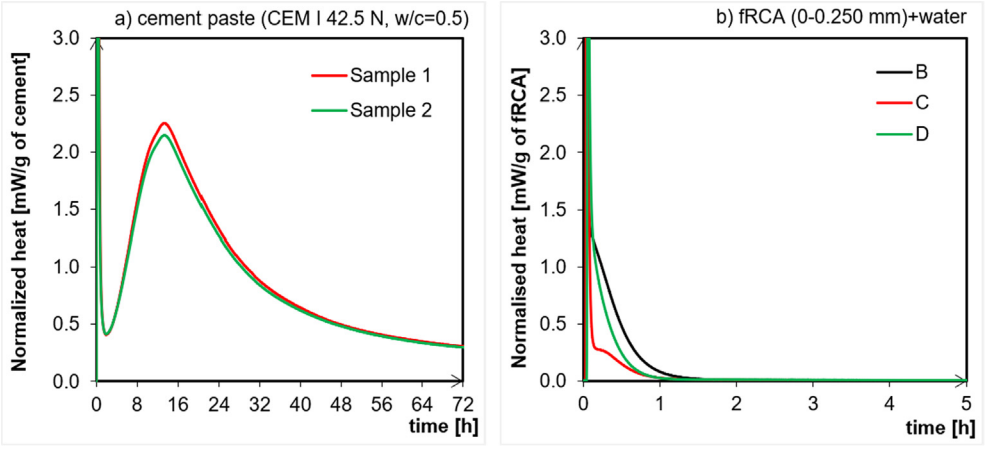

Fig. 12. Normalized heat for (a) cement paste (sample 1 and sample 2 are cement paste which was tested in duplo), (b) fRCA (0–0.250 mm) with water addition. The measurements are performed with three-channel TAM Air, Thermometric, in isothermal conditions (20 °C).

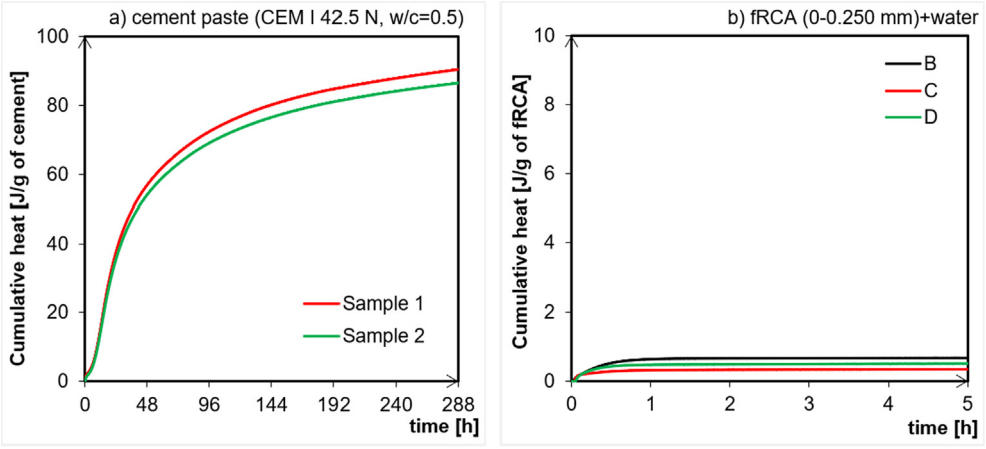

Fig. 13. Cumulative heat for (a) cement paste, (b) fRCA (0–0.250 mm) with water addition.

Particle shape. The fRCA particles are angular and elongated compared to round river sand. The angular shape and rough surface of fRCA particles result in more frictional resistance to the free flow and decreased packing of angular shapes vs. spherical shapes [46–48]. A maximization of the packing density of the particles can be achieved by adjusting the grading of the aggregates, consequently improving the overall performance of the concrete mix [11,49–51].

Particle size distribution. The fRCA (B, C, D) show different particle size distribution compared to river sand, mainly due to differ-

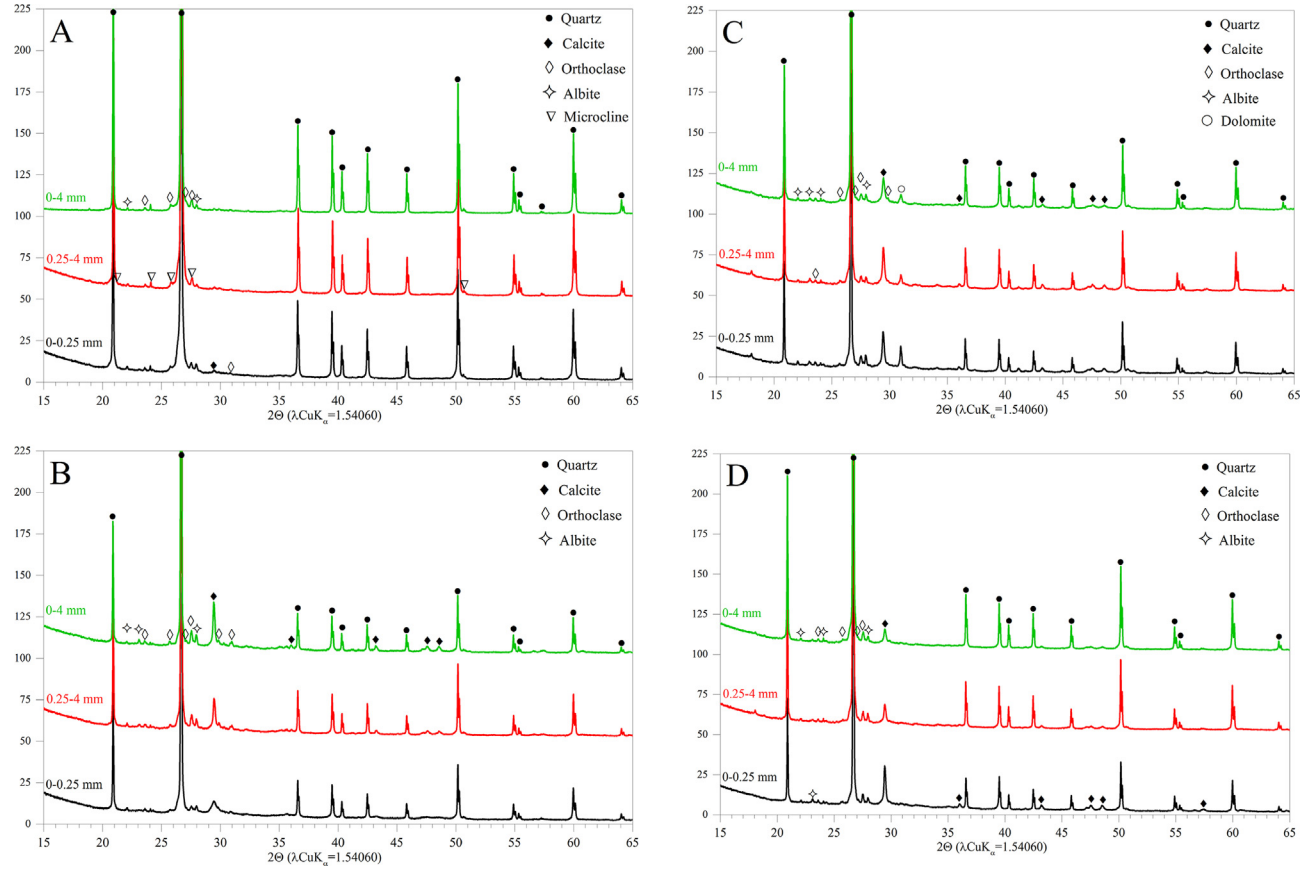

Fig. 14. X-ray diffractograms of the river sand (A) and fRCA (B, C, D).

Table 5
Phase quantification by Rietveld refinement method (wt.%).

Phase	Quartz	Albite	Orthoclase	Microcline	Calcite	Dolomite	Amorphous
A							
0–0.25 mm	91.1	2.9	1.3	3.9	0.0	0.0	0.9
0.25–4 mm	95.3	2.5	1.7	0.0	0.0	0.0	0.5
0–4 mm	94.1	1.5	0.8	3.2	0.0	0.0	0.4
B							
0–0.25 mm	58.8	3.5	3.7	0.0	8.6	0.0	25.3
0.25–4 mm	58.2	2.6	5.0	0.0	7.0	0.0	27.3
0–4 mm	57.7	3.6	4.9	0.0	8.7	0.0	25.1
C							
0–0.25 mm	48.5	4.1	4.1	0.0	9.6	3.4	30.4
0.25–4 mm	55.3	2.3	3.5	0.0	10.7	1.8	26.5
0–4 mm	62.7	3.0	4.7	0.0	7.6	0.0	21.9
D							
0–0.25 mm	50.1	3.2	3.1	0.0	9.8	0.0	33.8
0.25–4 mm	62.7	2.5	2.7	0.0	5.1	0.0	27.1
0–4 mm	72.1	2.4	2.6	0.0	3.8	0.0	19.0

ent content of the fine material (<0.250 mm). The impact of the fine material on the workability can be significant, depending on fRCA incorporation percentage. Therefore, it is important to control the particle size distribution of the fRCA within the grading limits for reference sand.

Content of fraction 0–0.250 mm. Increased amount of fines (particles < 0.250 mm) increases the required amount of water to wet the particle surfaces adequately and to maintain a specified workability. The content of fine material (<0.250 mm) also affects the aggregate particle packing and significantly diminish the effect of superplasticizers on normal concrete rheology (flow characteristics). Therefore, NEN-EN 206 in combination with NEN 8005:2017 [52], limits the content and prescribes minimum required quantity of fine material (< 0.250 mm) per m^3 of concrete depending on the largest grain size (D_{max}), more fines being required in concrete with lower D_{max}. This suggests that fRCA, with higher amounts of fine material (< 0.250 mm), is more suitable for concrete with lower D_{max}. As showed in Fig. 2, the amount of fine material (< 0.250 mm) in fRCA (C and D) is about two times higher than in river sand (A), except for B sand. The content of fine material (< 0.250 mm) for B sand is 6 wt.%, while for C and D sand these values are 15 wt.% and 18 wt.% respectively. When the fraction 0–0.250 mm is removed from fraction 0–4 mm, chemical and mineralogical differences between both fractions are marginal. This is

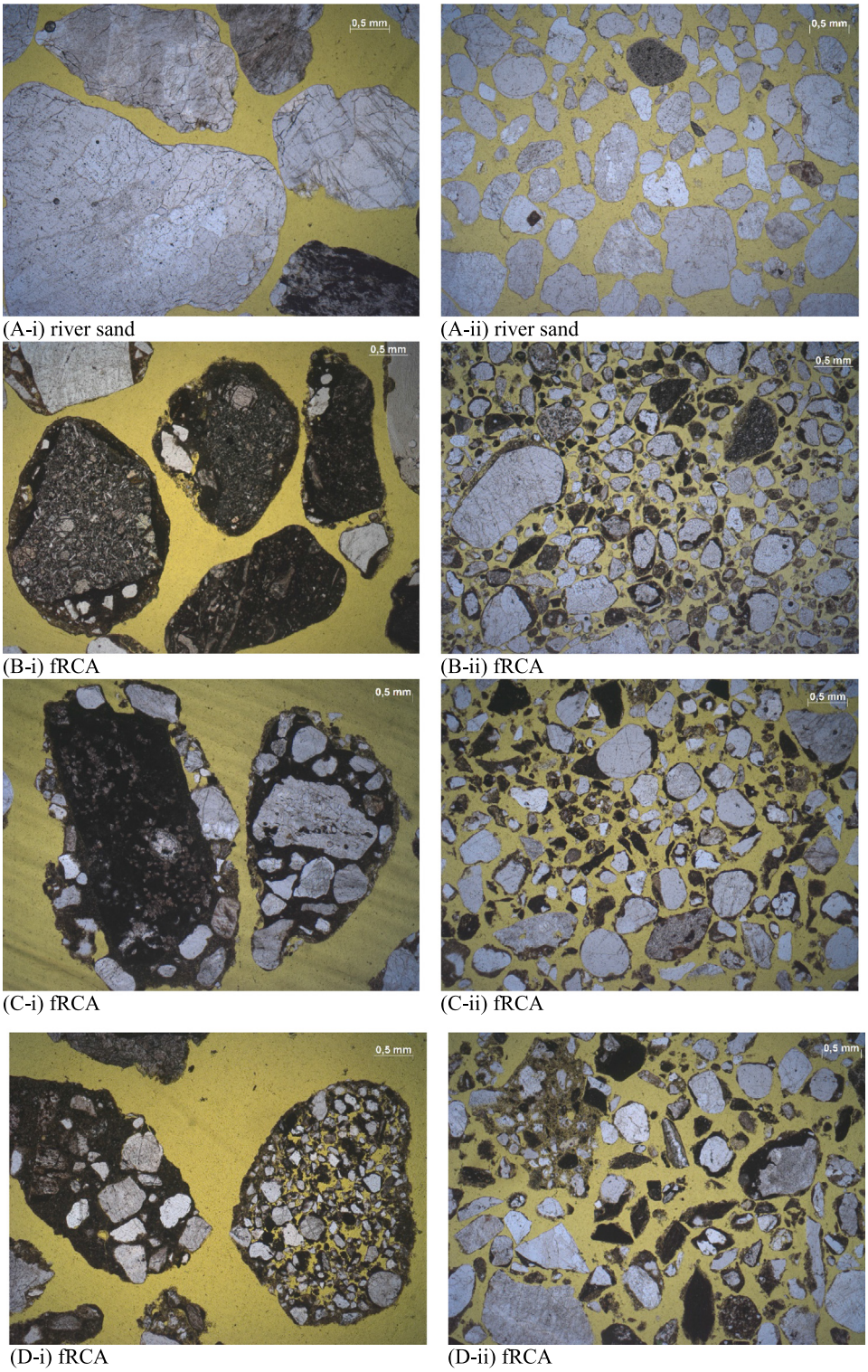

Fig. 15. Microphotographs showing examples of: (*i*) fraction 2–4 mm; (*ii*) fraction 0.063–2 mm in plane polarized light from different batches (A: river sand; B, C, D: different batches of fRCA).

due to the small part of fraction 0–0.250 mm which makes up of the total original fRCA fraction 0–4 mm (Fig. 2). The critical allowed content for fraction 0–0.250 mm in total fRCA fraction 0–4 mm should be established in the future.

Specific surface area (BET). The increased BET specific surface area of fRCA compared to river sand is caused by the presence of porous adhered cement paste. In general, the porosity of cement paste can differ significantly, depending on the amount of paste, type of used cement, content of remaining reaction products [53], and carbonation of paste. For instance, carbonation makes CEM I-based binder less porous, while CEM III/B-based binder more porous [54]. The values of surface areas of studied fRCA are comparable to results of Bendimerad et al. [35], who found BET surfaces of 5.3 m^2/g and 9.9 m^2/g for the sand (0–4 mm) and fine

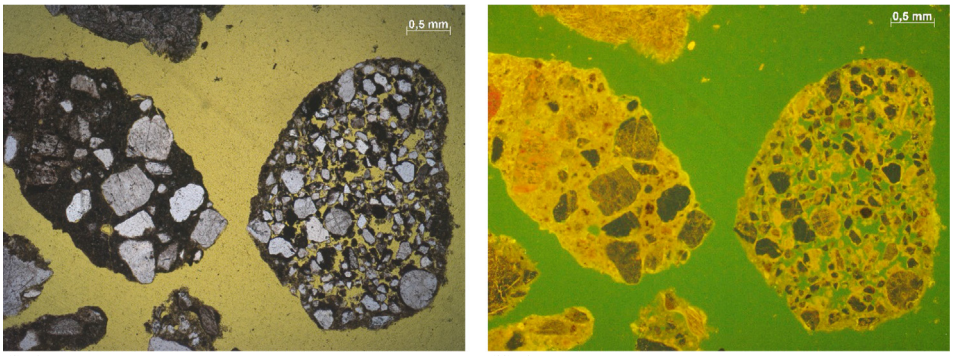

(i) fRCA D (ii) fRCA D

Fig. 16. Microphotographs showing type III (left) and IV (right) particles of the fraction 2–4 mm in fRCA D, in: (i) plane polarized light, ii) under UV light.

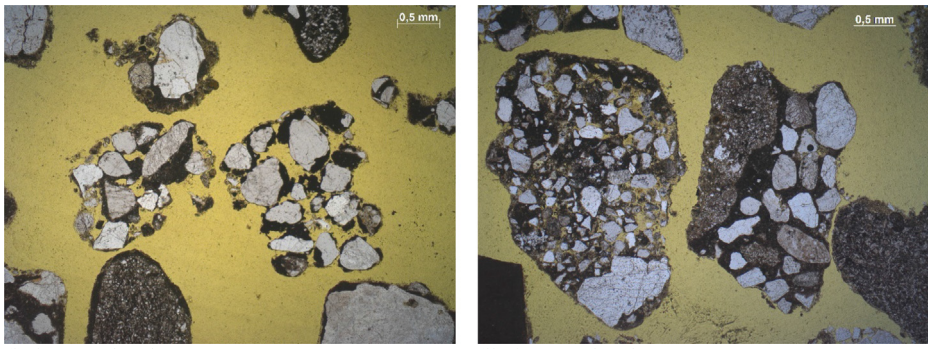

(i) fRCA B batch (ii) fRCA D batch

Fig. 17. Microphotographs of type IV (left) and type III (right) particles.

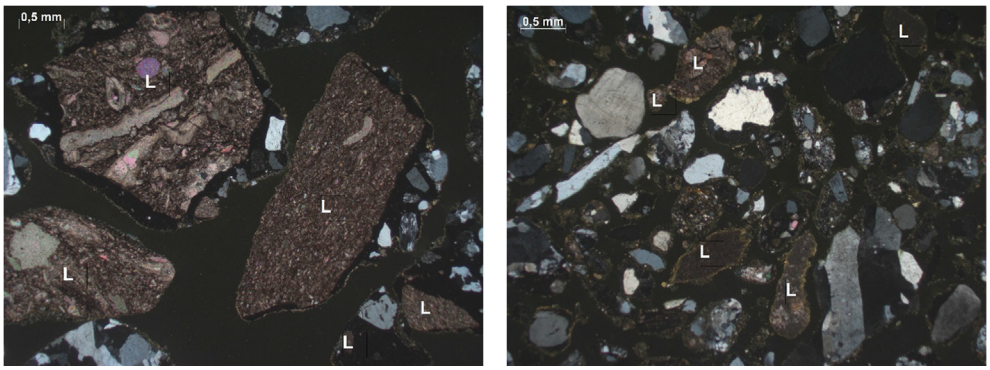

Fig. 18. Microphotographs of limestone (L) aggregate particles in B batch fraction 2–4 mm (left) and D batch fraction 0.063–2 mm (right) in cross polarized light.

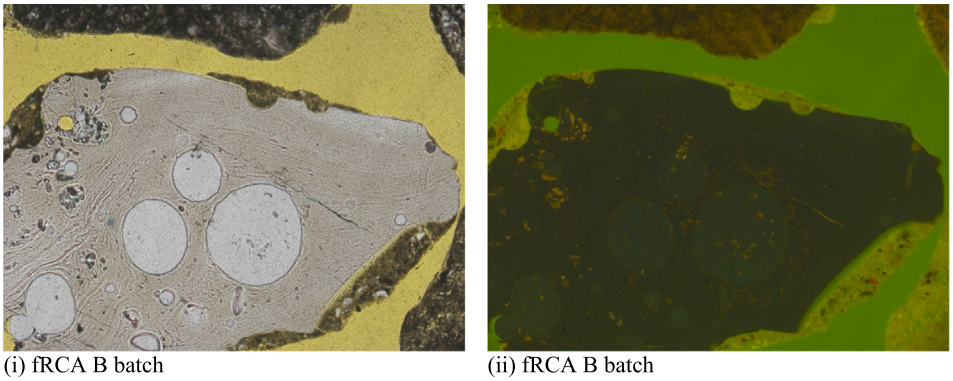

(i) fRCA B batch (ii) fRCA B batch

Fig. 19. Microphotographs of an interfacial crack in fRCA B (i) plane polarized light and (ii) UV light.

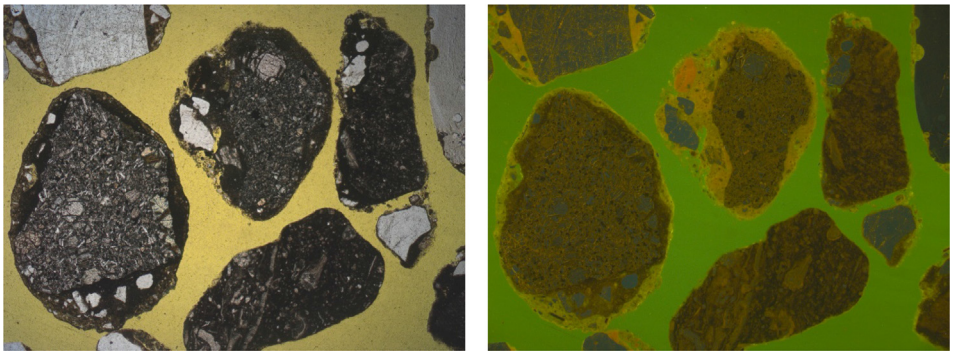

(i) fRCA B batch (ii) fRCA B batch

Fig. 20. Microphotographs of fRCA B particles without interface cracks:(i) plane polarized light, (ii) UV light.

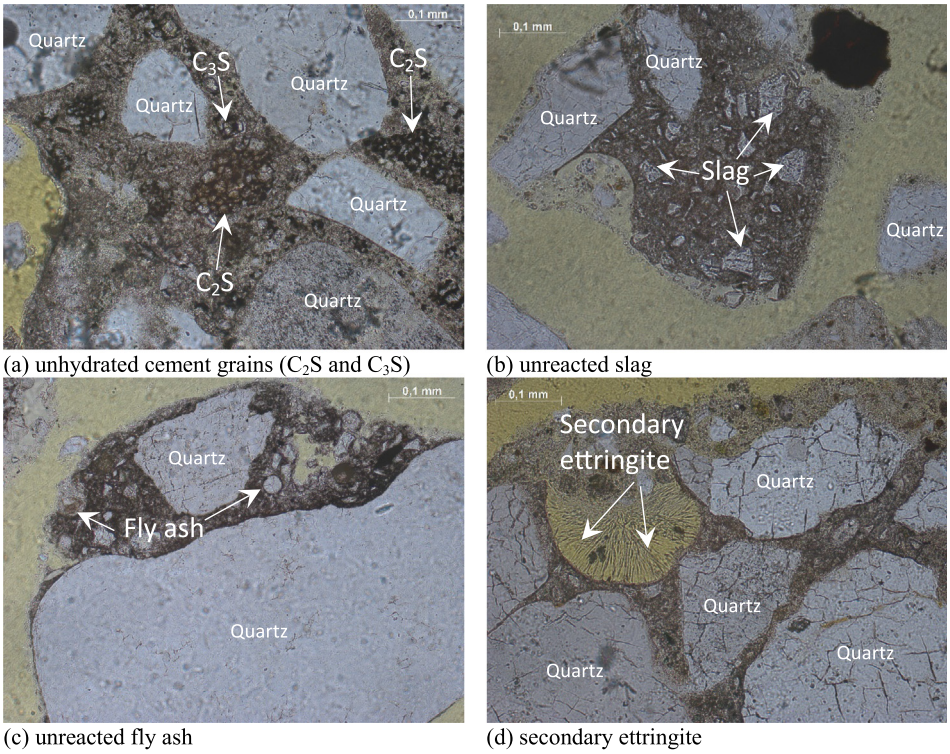

(a) unhydrated cement grains (C_2S and C_3S) (b) unreacted slag

(c) unreacted fly ash (d) secondary ettringite

Fig. 21. Microphotographs showing (a) residual unhydrated cement grains (C_2S and C_3S) in old cement paste (C batch); (b) unreacted ground granulated blast furnace slag in old cement paste (C batch); (c) unreacted fly ash in old cement paste (C batch); (d) air void partly filled by secondary ettringite (D batch) in plane polarized light.

(<63 μm) fractions, respectively. An increase of surface area and greater significance of short-range, weak forces between the smaller particles below approximately 100 μm [55] will result in a decrease of packing density. The increased surface area of fRCA would also require more water to wet and more paste to coat and lubricate the aggregate particles. This has been observed previously by others [35] and it has been suggested that the effective water intended for the cement paste might be attracted and kept in the menisci created by the recycled fines. Therefore, the bleeding water might be lower than in the control mix and the plastic shrinkage related to insufficient curing may increase [35]. In that case relatively more water is necessary to overcome the curing.

Water absorption of fRCA. Results also show a considerably higher water absorption of fRCA than river sand. This is the sum of water absorption of original aggregate particles and water absorption of residual cement paste or mortar around them. The densities from helium pycnometry (Fig. 8) and water absorption (Fig. 9) are comparable amongst different fRCA, although content of old cement paste and surface areas differ. This is contrary to what could be expected. Results in literature are differing. Whereas Zhao et al. [56] reported that the water absorption of fRCA is linearly proportional to the content of the old cement paste, Belin et al. [53] showed that two recycled concrete aggregate types with similar 24 h absorption values can have very different absorption kinetics. Rather than the amount of old cement paste present, its properties, like size, morphology and porosity, may explain the differences in water absorption [56]. PFM showed clear differences among these properties, which are to some extent determined by the original mix design(s) like water-to-cement ratio. The high water absorption of fRCA may have a detrimental effect since it affects concrete workability while it can have a beneficial effect when the fRCA is considered as internal water source for shrinkage

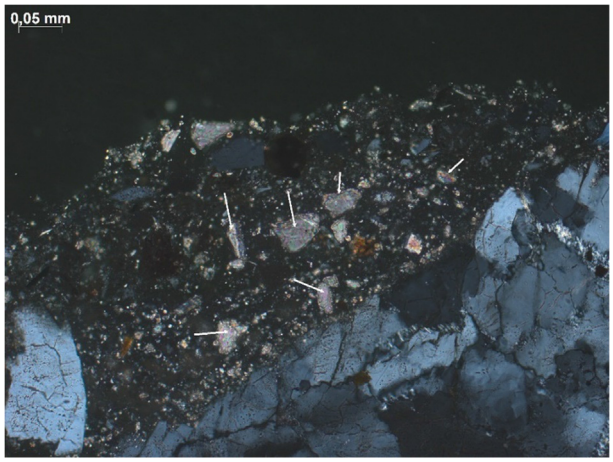

Fig. 22. Microphotograph showing limestone filler (indicated by white arrows) in B batch, in cross polarized light.

prevention. The high water absorption of the fRCA requires that the water absorbed by these aggregates is compensated by extra water during the mixing process [57].

Cl^- and SO_4^{2-} content. For all fRCA, the water soluble sulfate content according to NEN-EN 1744–1:2009+A1:2012 (Table 2) is lower than the total amount of sulfate calculated from XRF (Table 3). This implies that either part of the sulfate present in fRCA is insoluble or present as sulfide. Regarding chlorides, total chloride contents according to NEN-EN 1744–5:2006 [23] (Table 2) and XRF (Table 3) are in the similar order of magnitude; variations may be due to differences in testing method and preparation (including grinding) for analysis. The chemical analysis showed that all the samples had acid-soluble chlorides up to 0.04 % and water-soluble sulfates up to 0.37 %. Given the acceptance criteria of NEN 12620:2002 +A1:2008 [30] for recycled concrete aggregates, all investigated samples with particle range 0–4 mm, can be used in structural concrete.

Mineralogical composition of fRCA. Dutch concrete aggregates are typically river or marine sand and gravel, with a dominantly siliceous composition, i.e. monomineralic quartz and (impure) sandstone with minor (in river aggregate) to significant (in marine aggregate) chert. The minor constituents may be limestone or some volcanic rocks such as basalt. The fRCA is typically a blend of aggregates from different sources, possibly reflecting regional differences in aggregate and filler sources and cement types used. The original aggregate in the studied fRCA is also dominantly siliceous (Tables 3, 5 and Fig. 15). Other components, such as CaO, Al_2O_3, Fe_2O_3 and MgO, reflect either differences in original aggregate composition, such as the presence of (dolomitic) limestone in the aggregate, and/or relative amounts of binders present in the adhering cement paste (e.g. CEM I vs. CEM III/B). The chemical composition of the 0–4 mm fraction of studied fRCA D is similar to that of the fraction 0–4 mm studied by Lotfi and Rem [37], which was obtained from Dutch recycled concrete based on the use of CEM III/B cement. Different results from other studies [3,58] illustrate the mentioned role of parent concrete origin. PFM showed minor amounts of clinkers, SCMs (slag, fly ash) and some secondary ettringite in old cement paste. The mineral composition and surface microstructure of the fRCA will affect the growth of new hydration products and the bonding between the new and old cement matrices, which might affect the mechanical properties of new mortars/concretes with fRCA. Substantial content of carbonates was measured for fRCA by TG-MS (Table 4) and XRD-Rietveld refinement (Table 5), especially for the specimens with particle range 0–0.250 mm. Microscopy shows that Ca-carbonates are present as original limestone filler and aggregate as well as carbonated cement paste (Section 3.3). Differences between TG-MS (Table 4) and XRD Rietveld refinement (Table 5) in terms of Ca-carbonates amount, may be due to the presence of amorphous or poorly crystalline $CaCO_3$ and Rietveld fitting parameters (possibly not suitable for all types of carbonates present).

Reactivity of unreacted binder particles. In general, the content and composition of adhered cement paste in fRCA will depend on the parent concrete (type of cement used in concrete, concrete water-to-cement ratio), recycling technique and storage of fRCA. PFM shows that unreacted binder particles such as clinkers or SCMs (slag, fly ash) are present in the adhered cement paste. The common presence of SCMs, in particular slag, is in accordance with type of cement commonly used in the Netherlands. In the Netherlands, slag cement represents over 70 % of the cement market share [59]. Whether the unreacted binder particles in studied fRCA still represent any reactivity may be doubted. Based on the calorimetry results (Fig. 13), the contribution of studied fRCA to heat development, was negligible. This might be due to low amount of unreacted binder particles, their fineness and their chemical and mineralogical composition. Although not identified within the XRD detection limit, unhydrated Portland clinkers (such as C_2S, C_3S) were found in minor amounts in the thin sections by PFM. Part of the clinker and SCMs particles were relatively coarse (e.g. diameter > 63 μm), which may both be due to the fact that the smaller ones have reacted and Portland clinker and slag were usually more coarse in the past. Cementitious reaction products (e.g. CSH) are considered to be nonreactive, unless thermally reactivated [60,61].

Milling time to complete crushing of different fractions 0–4 mm has shown that the milling of fRCA compared to the river sand is much faster. This parameter may help to determine the

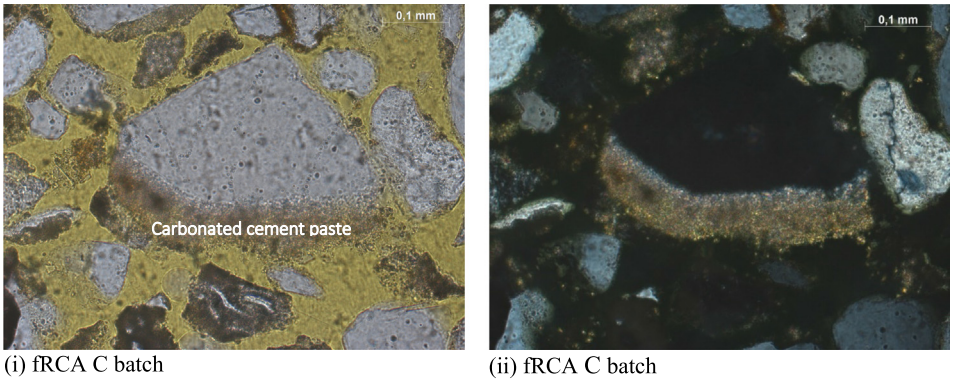

(i) fRCA C batch (ii) fRCA C batch

Fig. 23. Microphotograph showing a typical example of carbonated cement paste from the parent concrete (C batch), (*i*) in plane polarized light, (*ii*) in cross polarized light.

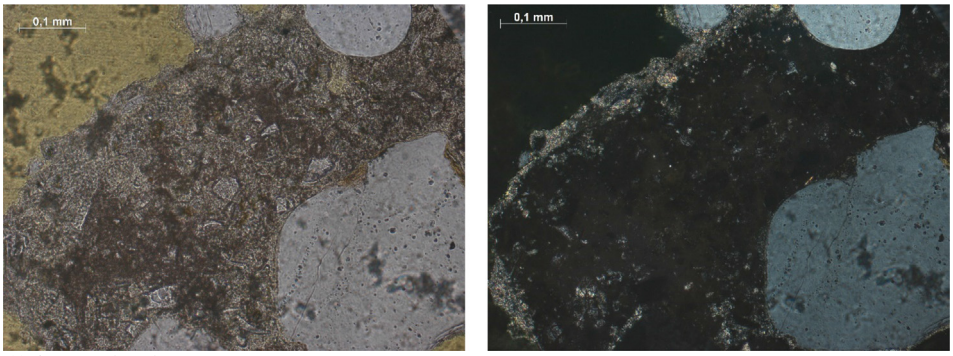

(i) fRCA C batch *(ii) fRCA C batch*

Fig. 24. Microphotograph showing a typical example of a thin carbonated outermost rim on a particle possible formed during storage (C batch) (*i*) in plane polarized light, (*ii*) in cross polarized light.

Table 6
Quality indicators for fRCA in relation to the concrete mix design.

Indicator	River sand (A)	fRCA (B, C, D)	concrete mix design
Particle shape	Round	Crushed	Packing density, workability
Particle size distribution	'S' shape curve	Linear cumulative curve	Packing density, water demand, workability
Content of fraction 0–0.250 mm	Max 5 wt.%	5–20 wt.%	Grading, workability
Density	2.65 g/cm^3	2.45 – 2.55 g/cm^3	Elastic modulus
Specific surface area (BET)	0.7 m^2/g	8.0 m^2/g	Water demand
Water absorption	1.0 %	7.0 %	Water demand
Cl^- and SO_4^{2-}	Very low	Low	Setting time,durability
Mineralogy	Quartz (95%), albite, orthoclase	Quartz (60%), albite, orthoclase, dolomite, calcite	Type of replacement
Cement paste content	0.00	~25.0 wt%	Water demand, use of superplasticizers, increased cement content
Milling time to complete crushing	40 min	5–15 min	Type of replacement

final application of the fRCA, such as type of substitution (sand, filler, binder). As milling time has indicated, the hardness of fRCA is low compared to river sand. It is believed that the high content of cement paste and angular particle shape of fRCA, enabled faster milling of fRCA compared to river sand.

Microcracking. A good interface between adhered cement paste and original parent concrete aggregates is essential to resist forces in the bond plane and it is important in determining mechanical and durability properties. Based on PFM observations, the presence of microcracks in the fRCA was negligible. Nevertheless, different ITZs will be present in microstructure of hardened mortars and concretes with fRCA due to compositional and porosity differences among fRCA.

The results implied that physical, chemical and mineralogical properties of fRCA are dependent on the parent concrete, recycling technique and storage of fRCA. Mixing of different types of construction materials at the recycling plant (e.g. traditional, ultra-high strength concrete, light- and heavyweight concretes, fiber reinforced concrete, etc.) which may have been exposed to different environmental conditions (under chloride ingress, carbonation, chemical attack, alkali–silica reaction, etc.), caused the compositional variations (SiO_2 and CaO) and levels of contamination (Cl- and SO_4^{2-} content) among investigated fRCA (Table 2 and Table 3). The way the fRCA are generated, will have a direct impact on the particle size distribution and quantity of the fines 0–0.250 mm, as demonstrated in Fig. 2 and Fig. 5. For instance, the increased number of crushing steps will increase the content of fine material (sand C and D have larger content of fraction 0–0.250 mm compared to sand B). The outdoor storage of fRCA causes carbonation of outer layers of sand piles, and agglomeration of the material. As shown in Fig. 1, agglomerates remain in sands C and D after drying.

The fRCA characterized by large mineral content, low contamination, negligible reactivity and low density reduction implies the potential of Dutch fRCA from different parent concretes to be used in the production of blended sands with similar performances to the natural sand. The findings provide guideline for selecting fRCA for concrete mix and support the broader utilization of fRCA in concrete in practical applications with reduced material cost and environmental impact. In the further studies, it will be investigated which parameters (quality indicators) govern workability and strength of mortars/concretes.

5. Conclusions

This study investigated the physical, chemical and mineralogical properties of Dutch fRCA from unknown concrete by means of multiple characterization techniques combined.

The following conclusions can be drawn based on this study:

(1) The amount of fine material (<0.250 mm) in fRCA (C and D) is about two times higher than in river sand (A), except for B sand. Similarly, their surface area was greatly increased compared to river sand. Even so, it was demonstrated that when fraction 0–0.250 mm is cut from the sand fraction 0–4 mm, the chemical and mineralogical differences between fractions 0.250–4 mm and 0–4 mm are marginal.
(2) The water absorption of fRCA was high and reduction of density was low, and their values were similar for different fRCA. Although the water absorption was similar, the water absorption kinetics of different fRCA is believed to be different due to the different morphologies of the cement patches at the surface of the grains. This assumption is based on the PFM observations, where the cement patches varied, from

smaller and thinner to larger and thicker. Microcracking was absent at the interface between adhered cement paste and original parent concrete aggregates.

(3) Although the content of the cement paste in fRCA was large (on average 22 wt.%), the content of chlorides was minor. In addition, the content of sulfates was below the critical values adopted for aggregates for use in reinforced concrete, with exception for fine fraction 0–0.250 mm. Therefore, from the aspect of contamination, the fRCA (0–4 mm) has large potential for sand replacement in new concrete.

(4) Based on XRD characterization of different fRCA, it was found that they are mainly made up by crystalline phases (>70 wt.%), notably quartz (>60 wt.%). PFM study supported XRD results and revealed minor minerals such as clinkers and secondary ettringite or distinguished between limestone aggregates and $CaCO_3$ formed by carbonation of cement paste. The fRCA (B, C, D) fractions (0–0.250 mm, 0.250–4 mm, 0–4 mm) show some differences in chemical composition, notably for SiO_2 and CaO contents. TG-MS analysis revealed minor amount of portlandite.

(5) Whether the unreacted binder particles in studied fRCA still represent any reactivity may be doubted. Based on the calorimetry results, the contribution of studied fRCA to heat development, was negligible. Cementitious reaction products (e.g. CSH) are considered to be nonreactive, unless thermally reactivated.

(6) This study suggests that the determination of the chemical composition can provide first line control regarding composition and potential contamination of fRCA. In addition, grading (particle size distribution) and water absorption (kinetics) should be measured. After that, it can be decided which additional tests are necessary (if necessary) to be done in order to evaluate the suitability of fRCA for replacement of natural fine aggregates in new concrete.

(7) Finally, the present work provides new insights for better understanding of the variations among different fRCA batches toward their use in the new concrete mix design. The framework in this study should be used to assess the characteristics of fRCA.

(8) Further study will use these characterization results to understand the effect of studied properties of different fRCA on the properties of mortars.

CRediT authorship contribution statement

Marija Nedeljković: Conceptualization, Methodology, Investigation, Writing - original draft, Visualization. **Jeanette Visser:** Conceptualization, Methodology, Writing - review & editing, Supervision. **Timo G. Nijland:** Methodology, Investigation, Writing - review & editing, Supervision. **Siska Valcke:** Methodology, Writing - review & editing, Funding acquisition. **Erik Schlangen:** Writing - review & editing, Supervision, Funding acquisition.

Declaration of Competing Interest

The authors declare that they have no known competing financial interests or personal relationships that could have appeared to influence the work reported in this paper.

Acknowledgements

Authors acknowledge funding provided by the Materials innovation institute M2i, Rijkswaterstaat, TNO, TweeR Recycling, AVG, Caron Recycling (CRH). Furthermore, the authors would like to acknowledge the material contribution (sample of fRCA) made by the recycling plants TweeR Recycling, AVG and Caron Recycling (CRH). The first author gratefully acknowledge Emanuele Rossi for valuable instructions and discussions related to isothermal calorimetry experiments. The authors thank Willem Duvalois for his help with XRD analysis, John van den Berg for his help with chemical analyses, Ron Lautz for his help with thin section preparations. The first author also acknowledge Wim Ekkelenkamp for valuable discussions related to concrete recycling and Martin Verweij for discussions related to cement recycling.

References

[1] A circular economy in the Netherlands by 2050. September 2016.
[2] N. Tošić, S. Marinković, T. Dašić, M. Stanić, Multicriteria optimization of natural and recycled aggregate concrete for structural use, J. Cleaner Prod. 87 (2015) 766–776, https://doi.org/10.1016/j.jclepro.2014.10.070.
[3] P.C.C. Gomes, C. Ulsen, F.A. Pereira, M. Quattrone, S.C. Angulo, Comminution and sizing processes of concrete block waste as recycled aggregates, Waste Manage. 45 (2015) 171–179, https://doi.org/10.1016/j.wasman.2015.07.008.
[4] S.C. Angulo, C. Ulsen, V.M. John, H. Kahn, M.A. Cincotto, Chemical–mineralogical characterization of C&D waste recycled aggregates from São Paulo, Brazil, Waste Manag. 29 (2) (2009) 721–730, https://doi.org/10.1016/j.wasman.2008.07.009.
[5] J. de Brito, F. Agrela, R.V. Silva, Legal regulations of recycled aggregate concrete in buildings and roads, In New Trends in Eco-efficient and Recycled Concrete, Woodhead Publishing, 2019, pp. 509-526.
[6] E. Vázquez (Ed.), Progress of recycling in the built environment: final report of the RILEM Technical Committee 217-PRE (Vol. 8), Springer Science & Business Media, 2012.
[7] J. Schoon, K. De Buysser, I. Van Driessche, N. De Belie, Fines extracted from recycled concrete as alternative raw material for Portland cement clinker production, Cem. Concr. Compos. 58 (2015) 70–80, https://doi.org/10.1016/j.cemconcomp.2015.01.003.
[8] C. Diliberto, A. Lecomte, J.M. Mechling, L. Izoret, A. Smith, Valorisation of recycled concrete sands in cement raw meal for cement production, Mater. Struct. 50 (2) (2017) 127, https://doi.org/10.1617/s11527-017-0996-8.
[9] I. Nováková, B.-A. Buyle, Sand Replacement by Fine Recycled Concrete Aggregates as an Approach for Sustainable Cementitious Materials, In Proceedings of the International Conference of Sustainable Production and Use of Cement and Concrete, Springer, 2020.
[10] M.E. Bouarroudj, S. Remond, F. Michel, Z. Zhao, D. Bulteel, L. Courard, Use of a reference limestone fine aggregate to study the fresh and hard behavior of mortar made with recycled fine aggregate, Mater. Struct. 52 (1) (2019) 18, https://doi.org/10.1617/s11527-019-1325-1.
[11] S. Fennis, Design of ecological concrete by particle packing optimization PhD thesis, Delft University of Technology, The Netherlands, 2011.
[12] R.B. Polder, M.R. De Rooij, Durability of marine concrete structures: field investigations and modelling, Heron 50 (3) (2005).
[13] C.Y. Ji, Y.Y. Chen, Y.Z. Chen, J.F. Zhuang, X.J. Chen, Lin, Effect of moisture state of recycled fine aggregate on the cracking resistibility of concrete, Constr. Build. Mater. 44 (2013) 726–733, https://doi.org/10.1016/j.conbuildmat.2013.03.059.
[14] A.Z. Bendimerad, E. Roziere, A. Loukili, Combined experimental methods to assess absorption rate of natural and recycled aggregates, Mater. Struct. 48 (11) (2015) 3557–3569, https://doi.org/10.1617/s11527-014-0421-5.
[15] T. Le, S. Remond, G. Le Saout, E. Garcia-Diaz, Fresh behavior of mortar based on recycled sand–Influence of moisture condition, Constr. Build. Mater. 106 (2016) 35–42, https://doi.org/10.1016/j.conbuildmat.2015.12.071.
[16] M.E. Sosa, L.E. Carrizo, C.J. Zega, Y.V. Zaccardi, Water absorption of fine recycled aggregates: effective determination by a method based on electrical conductivity, Mater. Struct. 51 (5) (2018) 127, https://doi.org/10.1617/s11527-018-1248-2.
[17] F. Rodrigues, M.T. Carvalho, L. Evangelista, J. De Brito, Physical–chemical and mineralogical characterization of fine aggregates from construction and demolition waste recycling plants, J. Cleaner Prod. 52 (2013) 438–445, https://doi.org/10.1016/j.jclepro.2013.02.023.
[18] L. Evangelista, M. Guedes, J. De Brito, A.C. Ferro, M.F. Pereira, Physical, chemical and mineralogical properties of fine recycled aggregates made from concrete waste, Constr. Build. Mater. 86 (2015) 178–188, https://doi.org/10.1016/j.conbuildmat.2015.03.112.
[19] E.P. Barrett, L.G. Joyner, P.P. Halenda, The determination of pore volume and area distributions in porous substances. I. Computations from nitrogen isotherms, J. Am. Chem. Soc. 73 (1) (1951) 373–380.
[20] NEN-EN 1097-5:2008 en, in Test for mechanical and physical properties of aggregates - Part 5: Determination of the water content by drying in a ventilated oven. 2008.
[21] NEN-EN 1097-6:2013 en, in Tests for mechanical and physical properties of aggregates - Part 6: Determination of particle density and water absorption. 2013.
[22] NEN-EN 932-2:1999 en, in Tests for general properties of aggregates - Part 2: Methods for reducing laboratory samples. 1999.
[23] NEN-EN 1744-5:2006 en, in Tests for chemical properties of aggregates - Part 5: Determination of acid soluble chloride salts. 2006.

[24] NEN-EN 1744-1:2009+A1:2012 en, in Tests for chemical properties of aggregates - Part 1: Chemical analysis. 2009.
[25] NEN-EN 15169:2007 en, in Characterization of waste - Determination of loss on ignition in waste, sludge and sediments. 2007.
[26] M. Nedeljković, Carbonation mechanism of alkali-activated fly ash and slag materials: In view of long-term performance predictions PhD thesis, Delft University of Technology, The Netherlands, 2019.
[27] T. Nijland, J. Larbi, Microscopic examination of deteriorated concrete, in Non-destructive evaluation of reinforced concrete structures. 2010, Elsevier. p. 137-179.
[28] CURNET, Measures to prevent concrete damage due to alkali-silica reaction (ASR). CUR recommendation 89 (in Dutch). 2017: Gouda, the Netherlands.
[29] M.C. Powers, A new roundness scale for sedimentary particles, J. Sediment. Res. 23 (2) (1953) 117–119, https://doi.org/10.1306/D4269567-2B26-11D7-8648000102C1865D.
[30] NEN-EN 12620:2002+A1:2008 en, in Aggregates for concrete. 2008.
[31] X. Ouyang, Filler-Hydrates Adhesion Properties in Cement Paste System: Development of Sustainable Building Materials PhD thesis, Delft University of Technology, The Netherlands, 2017.
[32] M. Nedeljković, Z. Li, G. Ye, Setting, strength, and autogenous shrinkage of alkali-activated fly ash and slag pastes: Effect of slag content, Materials 11 (11) (2018) 2121, https://doi.org/10.3390/ma11112121.
[33] S. Zhang, Waste glass as partial binder precursor and fine aggregate replacement in alkali activated slag/fly ash system MSc thesis, Delft University of Technology, The Netherlands, 2015.
[34] Z. Li, M. Nedeljković, B. Chen, G. Ye, Mitigating the autogenous shrinkage of alkali-activated slag by metakaolin, Cem. Concr. Res. 122 (2019) 30–41, https://doi.org/10.1016/j.cemconres.2019.04.016.
[35] A.Z. Bendimerad, E. Rozière, A. Loukili, Plastic shrinkage and cracking risk of recycled aggregates concrete, Constr. Build. Mater. 121 (2016) 733–745, https://doi.org/10.1016/j.conbuildmat.2016.06.056.
[36] J.J. Beaudoin, V.S. Ramachandran, R.F. Feldman, Interaction of chloride and C-S-H, Cem. Concr. Res. 20 (6) (1990) 875–883, https://doi.org/10.1016/0008-8846(90)90049-4.
[37] S. Lotfi, P. Rem, Recycling of end of life concrete fines into hardened cement and clean sand, J. Environ. Prot. 7 (06) (2016) 934–950, https://doi.org/10.4236/jep.2016.76083.
[38] C. Ulsen, H. Kahn, G. Hawlitschek, E.A. Masini, S.C. Angulo, V.M. John, Production of recycled sand from construction and demolition waste, Constr. Build. Mater. 40 (2013) 1168–1173, https://doi.org/10.1016/j.conbuildmat.2012.02.004.
[39] H. Brocken, T.G. Nijland, White efflorescence on brick masonry and concrete masonry blocks, with special emphasis on sulfate efflorescence on concrete blocks, Constr. Build. Mater. 18 (5) (2004) 315–323, https://doi.org/10.1016/j.conbuildmat.2004.02.004.
[40] J.B. Odelson, E.A. Kerr, W. Vichit-Vadakan, Young's modulus of cement paste at elevated temperatures, Cem. Concr. Res. 37 (2) (2007) 258–263, https://doi.org/10.1016/j.cemconres.2006.11.006.
[41] C. Jiang, J. Fang, J.Y. Chen, X.L. Gu, Modeling the instantaneous phase composition of cement pastes under elevated temperatures, Cem. Concr. Res. 130 (2020), https://doi.org/10.1016/j.cemconres.2020.105987 105987.
[42] L. Evangelista, J. De Brito, Durability performance of concrete made with fine recycled concrete aggregates, Cem. Concr. Compos. 32 (1) (2010) 9–14, https://doi.org/10.1016/j.cemconcomp.2009.09.005.
[43] C.J. Zega, Á.A. Di Maio, Use of recycled fine aggregate in concretes with durable requirements, Waste Manage. 31 (11) (2011) 2336–2340, https://doi.org/10.1016/j.wasman.2011.06.011.
[44] P. Pereira, L. Evangelista, J. De Brito, The effect of superplasticisers on the workability and compressive strength of concrete made with fine recycled concrete aggregates, Constr. Build. Mater. 28 (1) (2012) 722–729, https://doi.org/10.1016/j.conbuildmat.2011.10.050.
[45] A.G. Khoshkenari, P. Shafigh, M. Moghimi, H.B. Mahmud, The role of 0–2 mm fine recycled concrete aggregate on the compressive and splitting tensile strengths of recycled concrete aggregate concrete, Mater. Des. 64 (2014) 345–354, https://doi.org/10.1016/j.matdes.2014.07.048.
[46] M. Behera, A.K. Minocha, S.K. Bhattacharyya, Flow behavior, microstructure, strength and shrinkage properties of self-compacting concrete incorporating recycled fine aggregate, Constr. Build. Mater. 228 (2019), https://doi.org/10.1016/j.conbuildmat.2019.116819 116819.
[47] N. Peronius, T. Sweeting, On the correlation of minimum porosity with particle size distribution, Powder Technol. 42 (2) (1985) 113–121, https://doi.org/10.1016/0032-5910(85)80043-7.
[48] J. Jiang, W. Zhou, Y. Gao, L. Wang, F. Wang, H.Y. Chu, G. Xu, B. Vandevyvere, Z. Sierens, J. Li, Feasibility of manufacturing ultra-high performance cement-based composites (UHPCCs) with recycled sand: A preliminary study, Waste Manage. 83 (2019) 104–112, https://doi.org/10.1016/j.wasman.2018.11.005.
[49] A.K.H. Kwan, W.W.S. Fung, Packing density measurement and modelling of fine aggregate and mortar, Cem. Concr. Compos. 31 (6) (2009) 349–357, https://doi.org/10.1016/j.cemconcomp.2009.03.006.
[50] P. Nanthagopalan, M. Haist, M. Santhanam, H.S. Müller, Investigation on the influence of granular packing on the flow properties of cementitious suspensions, Cem. Concr. Compos. 30 (9) (2008) 763–768, https://doi.org/10.1016/j.cemconcomp.2008.06.005.
[51] G.C. Cho, J. Dodds, J.C. Santamarina, Particle shape effects on packing density, stiffness, and strength: natural and crushed sands, J. Geotech. Geoenviron. Eng. 132 (5) (2006) 591–602, https://doi.org/10.1061/(ASCE)1090-0241(2006)132:5(591).
[52] NEN-EN 206+NEN 8005:2017 nl, in Concrete - Specification, performance, production and conformity + Dutch supplement to NEN-EN 206. 2017.
[53] P. Belin, G. Habert, M. Thiery, N. Roussel, Cement paste content and water absorption of recycled concrete coarse aggregates, Mater. Struct. 47 (9) (2014) 1451–1465, https://doi.org/10.1617/s11527-013-0128-z.
[54] P. Holthuizen, Chloride ingress of carbonated blast furnace slag cement mortars MSc thesis, Delft University of Technology, The Netherlands, 2016.
[55] R.M. German, Particle packing characteristics, 1989.
[56] Z. Zhao, S. Remond, D. Damidot, W. Xu, Influence of hardened cement paste content on the water absorption of fine recycled concrete aggregates, J. Sustain. Cem. Based Mater. 2 (3–4) (2013) 186–203, https://doi.org/10.1080/21650373.2013.812942.
[57] F. Cartuxo, J. De Brito, L. Evangelista, J.R. Jimenez, E.F. Ledesma, Rheological behaviour of concrete made with fine recycled concrete aggregates–Influence of the superplasticizer, Constr. Build. Mater. 89 (2015) 36–47, https://doi.org/10.1016/j.conbuildmat.2015.03.119.
[58] M.V.A. Florea, H.J.H. Brouwers, Properties of various size fractions of crushed concrete related to process conditions and re-use, Cem. Concr. Res. 52 (2013) 11–21, https://doi.org/10.1016/j.cemconres.2013.05.005.
[59] R. Kemp, E. Barteková, S. Türkeli, The innovation trajectory of eco-cement in the Netherlands: a co-evolution analysis, Int. Econ. Econ. Policy 14 (3) (2017) 409–429, https://doi.org/10.1007/s10368-017-0384-4.
[60] Z. Shui, D. Xuan, H. Wan, B. Cao, Rehydration reactivity of recycled mortar from concrete waste experienced to thermal treatment, Constr. Build. Mater. 22 (8) (2008) 1723–1729, https://doi.org/10.1016/j.conbuildmat.2007.05.012.
[61] Z. Shui, R. Yu, J. Dong, Activation of Fly Ash with Dehydrated Cement Paste, ACI Mater. J. 108 (2) (2011).